EURASIP Journal on Applied Signal Processing 2005:3, 252–272

Ultra-Wideband Radio

Robert A. Scholtz
Department of Electrical Engineering, University of Southern California, Los Angeles, CA 90089, USA
Email: scholtz@usc.edu

David M. Pozar
Department of Electrical and Computer Engineering, University of Massachusetts, Amherst, MA 01003, USA
Email: pozar@ecs.umass.edu

Won Namgoong
Department of Electrical Engineering, University of Southern California, Los Angeles, CA 90089, USA
Email: namgoong@usc.edu

Received 12 May 2004

The application of ultra-wideband (UWB) technology to low-cost short-range communications presents unique challenges to the communications engineer. The impact of the US FCC's regulations and the characteristics of the low-power UWB propagation channels are explored, and their effects on UWB hardware design are illustrated. This tutorial introduction includes references to more detailed explorations of the subject.

Keywords and phrases: UWB radio, UWB propagation, UWB antennas, UWB radio architectures, selective RAKE receivers, transmitted-reference receivers.

1. ORIGINS

It has been said that paradigm shifts in design and operation of systems are necessary to achieve orders-of-magnitude changes in performance. It would seem that such events have occurred in the world of radio communications with the advent of ultra-wideband (UWB) radio. Indeed, several remarkable innovations have taken place in the brief history of UWB radio. Initially transient analysis and time-domain measurements in microwave networks (1960s) and the patenting of *short-pulse* (often called *impulse* or *carrierless* or *baseband* or *UWB*) radio systems in the early 1970s were major departures from the then-current engineering practices. (For detailed descriptions of the early work in this field, see [1].) Marconi's view of using modulated sinusoidal carriers and high-Q filters for channelization has so dominated design and regulation of RF systems since the early twentieth century, that the viability of short-pulse systems often has been greeted with skepticism.

Bennett and Ross described the state of UWB engineering efforts near the end of the 1970s in a revealing paper.

> "BA[seband]R[adars] have been ... recently demonstrated for various applications, including auto precollision sensing, spaceship docking, airport surface traffic control, tanker ship docking, harbor collision avoidance, etc. These sensing applications cover ranges from 5 to 5000 ft ....
>
> Further applications resulted in the construction of a sub-nanosecond, single coaxial cable scheme for multiplexing data between computer terminals .... More recently baseband pulse techniques have been applied to the problem of developing a short-range wireless communication link. Here, the low EM pollution and covertness of operation potentially provide the means for wireless transmission without licensing." (From the Abstract of C. L. Bennett and G. F. Ross, Time-domain electromagnetics and its applications, *Proc. IEEE*, March 1978.)

The early applications of UWB technology were primarily radar related, driven by the promise of fine-range resolution that comes with large bandwidth. In the early 1990s, conferences on UWB technology were initiated and proceedings documented in book form [2, 3, 4, 5, 6, 7]. For the most part, the papers at these conferences are motivated by radar applications.

Table 1: Categories of applications approved by the FCC [8].

Class/application	Frequency band for operation at part 1 limit	User limitations
Communications and measurement systems	3.1 to 10.6 GHz (different out-of-band emission limits for indoor and outdoor devices)	No
Imaging: ground penetrating radar, wall, medical imaging	< 960 MHz or 3.1 to 10.6 GHz	Yes
Imaging: through wall	< 960 MHz or 1.99 to 10.6 GHz	Yes
Imaging: surveillance	1.99 to 10.6 GHz	Yes
Vehicular	24 to 29 GHz	No

Beginning in the late 1980s, small companies, for example, Multispectral Solutions, Inc. (http://www.multispectral.com/history.html), Pulson Communications (later to become Time Domain Corporation), and Aether Wire and Location (http://www.aetherwire.com), specializing in UWB technology, started basic research and development on communications and positioning systems. By the mid-1990s, when the UltRa Lab at the University of Southern California was formed (http://ultra.usc.edu/New_Site/), lobbying the US Federal Communications Commission (FCC) to allow UWB technology to be commercialized was beginning. At a US Army Research Office/UltRa Lab-Sponsored Workshop in May 1998, an FCC representative indicated that a notice of inquiry (NOI) into UWB was imminent, and the companies working on UWB technology decided to band together in an informal industry association now known as the Ultra-Wideband Working Group (http://www.uwb.org). The objective of this association was to convince the FCC to render a ruling favorable to the commercialization of UWB radio systems.

The FCC issued the NOI in September 1998 and within a year the Time Domain Corporation, US Radar, and Zircon Corporation had received waivers from the FCC to allow limited deployment of a small number of UWB devices to support continued development of the technology, and USC's UltRa Lab had an experimental license to study UWB radio transmissions. A notice of proposed rule making was issued in May 2000. In April 2002, after extensive commentary from industry, the FCC issued its first report and order on UWB technology, thereby providing regulations to support deployment of UWB radio systems. This FCC action was a major change in the approach to the regulation of RF emissions, allowing a significant portion of the RF spectrum, originally allocated in many smaller bands exclusively for specific uses, to be effectively shared with low-power UWB radios.

The FCC regulations classify UWB applications into several categories (see Table 1) with different emission regulations in each case. Maximum emissions in the prescribed bands are at an effective isotropic radiated power (EIRP) of −41.3 dBm per MHz, and the −10 dB level of the emissions must fall within the prescribed band (see Figure 1). In addition, for a radiator to be considered UWB, the 10 dB bandwidth $f_H - f_L$ must be at least 500 MHz, and the fractional bandwidth, $2(f_H - f_L)/(f_H + f_L)$, must be at least 0.2, as determined by the −10 dB power points f_H and f_L (see [8, paragraph 30]). UWB modulations are not prescribed by this regulation to be short pulse in nature, but it is noteworthy that testing of swept or stepped frequency systems must be determined with the sweep or step process turned off, making compliance unlikely (see [8, paragraph 32]). Devices satisfying the adopted UWB communication regulations will be allowed to operate on an unlicensed basis, fulfilling the potential noted by Bennett and Ross in 1978.

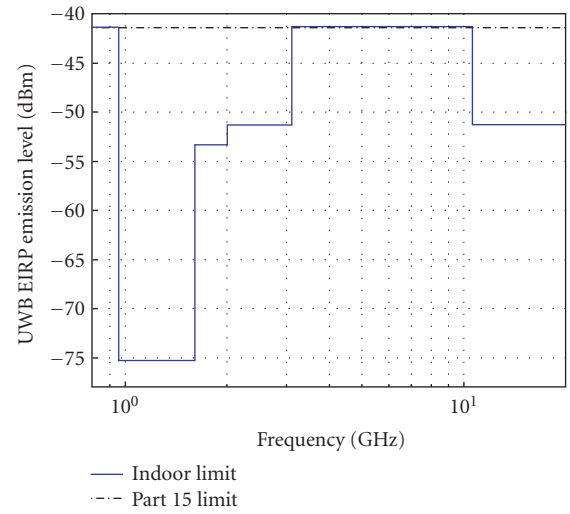

Figure 1: FCC's spectral mask for indoor communications applications [8], specifying measurements in a 1 MHz band. Different masks are used for different application categories.

A further FCC memorandum opinion and order and further notice of proposed rule making [9] "does not make any significant changes to the now-existing UWB technical parameters."

2. OVERVIEW OF UNIQUE FEATURES AND ISSUES

Communication engineers know that there are several compelling advantages to having more RF bandwidth. In all of the cases below, increasing RF bandwidth improves a desirable property.[1] Many assumptions and simplifications are hidden in these relations that may be difficult to justify rigorously for

[1]Note that the gross bandwidth parameter B_{RF} used in the relations of this section is defined differently in each case, and numerical values of one bandwidth measure cannot legitimately be substituted for another bandwidth measure when performing high-level tradeoffs [10].

UWB systems. For example, antennas behave like direction-sensitive filters over ultra-wide bandwidths, and the signal driving the transmitting antenna, the electric far field (even in free space), and the signal across the receiver load may differ considerably in waveshape and spectral content. Ideally matched correlation receivers are difficult to realize.

2.1. AWGN channel capacity and bandwidth efficiency

The channel capacity C (in bits per second (bps)) of the band-limited additive white Gaussian noise (AWGN) channel increases with RF bandwidth:

$$C = B_{\mathrm{RF}} \log_2 \left(1 + \frac{P_{\mathrm{rec}}}{B_{\mathrm{RF}} N_0}\right), \tag{1}$$

where B_{RF} is the RF bandwidth of the channel, P_{rec} is the received signal power, and N_0 is the noise power spectral density (PSD) in the RF bandwidth of the radio (see, e.g., [11, Section 5.5]). This equation is based on an idealized rectangular RF filter of width B_{RF} and does not account for many effects in real systems, including interference of all sorts, receiver mismatch, and so forth. In the event that the noise in the radio receiver is Gaussian but not white, Shannon's water filling theorem [12] indicates that capacity should in most circumstances increase with increased bandwidth under a fixed received power constraint. It also suggests that the distribution of power which achieves capacity in the band-limited AWGN channel corresponds to a flat PSD across the available frequency band.

2.2. Interference in UWB receivers

There is no doubt that UWB radios will be sharing the environment with other radio systems, some possibly creating UWB multiple access interference, and others creating narrowband interference in the UWB radio bands. The FCC regulations have set conditions that limit the interference from UWB radiators to other radio systems, by limiting UWB radios' EIRP in any 1 MHz band to -41.3 dBm. However, the issue of eliminating interference to UWB radios from other radiating systems is left to the ingenuity of the UWB radio designer. At least three standard bandwidth-related approaches to the handling of interference are possible, namely, spread-spectrum processing, interference excision, and selectable channelization. A back-of-the-envelope computation of the effects of these kinds of processing can be accomplished under the assumption that a reasonable model for the signal in the receiver is the sum of three terms: the desired signal with power P_{rec} uniformly spread over the RF bandwidth B_{RF}, an equivalent receiver noise with power density N_0, and a statistically independent interfering signal with power I occupying a fraction $1 - F$ of the RF bandwidth.

(i) *Spread-spectrum processing* works by using transmitted waveforms that span the available RF bandwidth B_{RF} as uniformly as possible, the RF bandwidth typically being much larger than the data bandwidth B_{data}. In the process of ideal correlation reception, the received signal is despread and the data recovered within a bandwidth B_{data} at a rate R_{data}, while at the same time, any interference power I is spread more or less uniformly across the RF bandwidth [13] in a noise-like manner. The data detector recovers all of the signal power, but the total noise PSD within the data bandwidth increases from N_0 to $N_0 + (I/B_{\mathrm{RF}})$. Hence, the effective energy-per-bit-to-noise density ratio is approximately

$$\left(\frac{E_{\mathrm{b}}}{N_{\mathrm{tot}}}\right)_{\mathrm{ss}} = \frac{P_{\mathrm{rec}}/R_{\mathrm{data}}}{N_0 + I/B_{\mathrm{RF}}}. \tag{2}$$

A more detailed performance computation based on spread-spectrum processing for interference mitigation in UWB radios is given in [14].

(ii) *Interference excision* works by filtering out (rejecting) narrowband interference. Assuming that the received waveform uniformly spans the available RF bandwidth and that the interfering signal can be eliminated by ideal notch filtering that removes a fraction $1 - F$ of the RF bandwidth, the noise power density in the remaining bandwidth FB_{RF} is N_0 and the remaining signal power is FP_{rec}. Hence, the effective energy-per-bit-to-noise density ratio for ideal interference excision is approximately

$$\left(\frac{E_{\mathrm{b}}}{N_{\mathrm{tot}}}\right)_{\mathrm{int\ ex}} = \frac{FP_{\mathrm{rec}}/R_{\mathrm{data}}}{N_0}. \tag{3}$$

Thus the primary effect of interference excision, in addition to removing the interfering signal, is to reduce the rate at which the receiver accumulates desired signal energy by a factor F.

(iii) *Selectable channelization* is a form of interference excision in which the RF bandwidth is divided into K approximately nonoverlapping subchannels, and only those subchannels without significant interference are processed to detect the transmitted data signal. This system is equivalent to signal excision with a bank of fixed filters, each of bandwidth B_{RF}/K. When the interference bandwidth fraction $1 - F$ is less than $1/K$, then excision of the interference can be accomplished by not processing one or two subchannels. In either case, the aggregate signal-to-noise power ratio is the same as that for signal excision, but the rate at which the receiver accumulates desired signal energy is reduced by a factor $1/K$ or $2/K$ when $1 - F < 1/K$.

A similar comparison of the effective energy-per-bit-to-noise density ratios for spread-spectrum processing and interference excision yields

$$\left(\frac{E_{\mathrm{b}}}{N_{\mathrm{tot}}}\right)_{\mathrm{ss}} > \left(\frac{E_{\mathrm{b}}}{N_{\mathrm{tot}}}\right)_{\mathrm{int\ ex}} \iff \frac{1}{F} > \frac{N_0 + I/B_{\mathrm{RF}}}{N_0}. \tag{4}$$

Hence, the best processing technique is determined by comparing the increase in observation time required to accumulate a prescribed amount of signal energy when interference is excised to the increase in the receiver's total noise floor when spread-spectrum techniques are used. Typically when the remaining band fraction F is large, signal excision will be preferred, but when most of the band must be excised to eliminate the interference and F is small, then spread-spectrum processing will be preferred. The dilemma in either comparison is that the designer does not usually know the received interference power I and/or F a priori.

It is worth noting that as the RF bandwidth B_{RF} increases in a shared spectrum environment, the likelihood of having more in-band interferers may increase. Signal excision of some form may be necessary for narrowbands in which strong interference is normally expected, and spread-spectrum processing may be desirable to handle less predictable and weaker sources of interference. In this case, strong narrowband interference is first excised, and the remaining signal is subject to spread-spectrum processing. If the interference can be completely excised, there is no added benefit to the spread-spectrum processing.

2.3. Time resolution

The time resolution T_{res} of a matched receiver generally is on the order of the reciprocal of the RF Gabor (RMS) bandwidth B_{RF}:

$$T_{res} \approx \frac{1}{B_{RF}}. \tag{5}$$

This gives a corresponding range resolution in positioning systems on the order of c/B_{RF}, where c is the speed of light. This time-resolution measure is well known in radar circles as a measure of the width of the peak of a matched-filter response to a waveform of RMS bandwidth B_{RF}. Although Woodward's radar ambiguity function was developed for time and Doppler mismatch assessment of narrowband receiver performance, a corresponding application of this concept to UWB signals can be developed [15].

The small value of T_{res} also can cause problems for the system designer. For example, in an ideal AWGN baseband channel, the number of measurements used in acquiring synchronization in a straightforward manner (e.g., a serial or parallel search) is proportional to T_{unc}/T_{res}, where T_{unc} is the duration of the initial time uncertainty interval that must be searched in the acquisition process. Rapid acquisition techniques of various types (see, e.g., [17, Section 6.8]), which usually take advantage of some property of the signal design, have been devised to reduce this quantity to $\log_2(T_{unc}/T_{res})$. Whatever technique used in the acquisition process, increasing the RF bandwidth of the signal generally stresses the synchronization process.

Monostatic radars have the advantage of being able to access the same clock signals on transmit and receive. Communication systems must have similar clocks at the transmitter and receiver to provide timing structure for digital modulation and demodulation. Differences in these clock periods can be removed by voltage control in the sync-tracking mode of the receiver, but during the sync acquisition phase in the receiver, differences in the transmit and receive clocks can cause problems. If two such clocks start in synchronism and if the elapsed time until the clocks are out of synchronism by T_{res} is T_{co}, then the time over which correlations can be computed usefully is bounded by T_{co}. Hence the clock stability S in parts per million (ppm) required to do acquisition correlation computations over T_{co} is

$$S \approx \frac{T_{res}}{T_{co}} \times 10^6 \approx \frac{10^6}{B_{RF}T_{co}} \quad \text{(ppm)}. \tag{6}$$

Hence, for a specified correlation time T_{co}, perhaps determined by the requirement to collect specified amount of signal energy, increases in the RF bandwidth provide more severe constraints on oscillator stability S.

2.4. Adding ultra to wideband

A large RF bandwidth by itself does not imply that a system is UWB. The FCC definition that a UWB signal have a fractional bandwidth of at least 0.2 means that of all possible systems with the same bandwidth $f_H - f_L$, those qualified as UWB have the lowest center frequencies $(f_H + f_L)/2$. The relatively low-frequency band of UWB systems provides propagation advantages through many materials (see Figure 2) and motivates the imaging applications in the FCC regulations.

Large fractional bandwidths do cause implementation problems for system architectures, antennas, and circuits. However, these problems can be overcome. The fundamental parameters that control UWB radio design are the characteristics of the channel: propagation effects, interference, and regulatory constraints on transmission.

3. MODELING THE RF CHANNEL

UWB channels present problems that differ somewhat from their narrowband counterparts. We will first explore a few candidate antennas, and where analytically/computationally feasible, describe their distortion effects on the transmission of a Gaussian monocycle source over a free-space channel. The construction of a link budget for power or energy transmission over a free-space channel is then illustrated with both rigorous computations and Friis equation approximations. Then we use real measurements to illustrate the considerably more complicated UWB channel structure and a variety of indoor communication channels.

3.1. Antenna design for UWB radio systems

UWB radio systems are characterized by multioctave to multidecade frequency bandwidths, and are expected to transmit and receive baseband pulse waveforms with minimum loss and distortion. Both transmit and receive antennas can affect the faithful transmission of UWB signal waveforms because of the effects of impedance mismatch over the operating bandwidth, pulse distortion effects, and the dispersive effects of frequency-dependent antenna gains and spreading factors [18, 19, 20, 21]. Some of the desirable antenna characteristics for UWB radio systems are

(i) wide impedance bandwidth;
(ii) fixed-phase center over frequency;
(iii) high radiation efficiency.

Good impedance matching over the operating frequency band is desired to minimize reflection loss and to avoid pulse distortion. If the phase center (the point where spherical wave radiation effectively originates) of an antenna moves with frequency (as is the case with spiral, log periodic, and traveling wave antennas), pulse dispersion will occur.

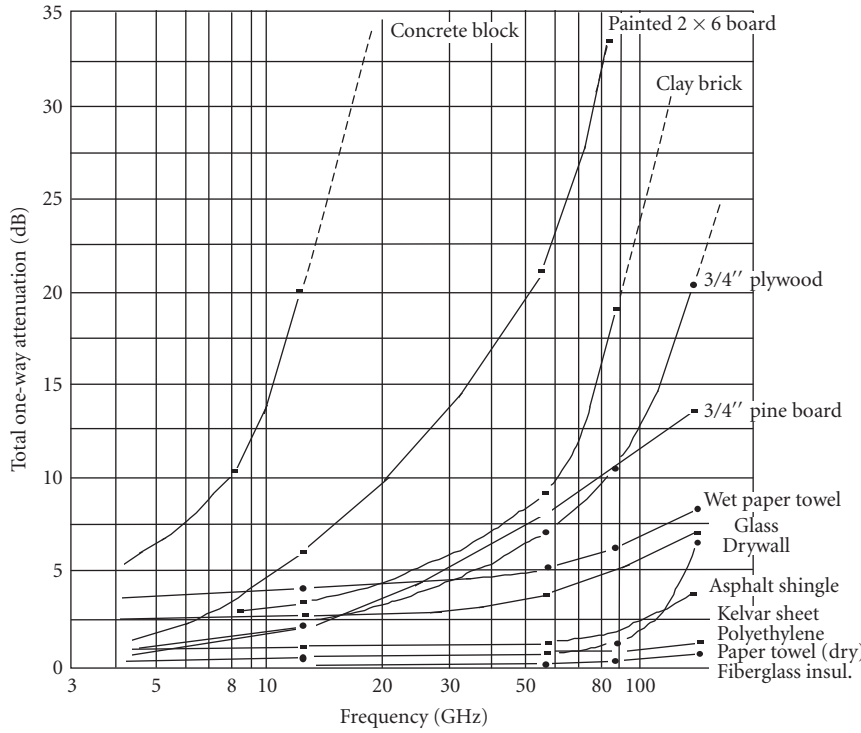

Figure 2: Total one-way attenuation through various materials (from [16] with the permission of the International Society for Optical Engineering (SPIE)).

Table 2: Some characteristics of antennas for UWB systems.

Antenna	Impedance bandwidth	Phase center stability	Radiation efficiency	Physical size
Dipole	Narrow	Good	High	Small
Loop	Narrow	Good	High	Small
Bow tie, diamond	Medium	Good	High	Medium
Vivaldi	Wide	Good	High	Large
LPDA	Wide	Poor	Medium	Large
Spiral	Wide	Poor	Medium	Large
Loaded dipole/loop	Medium	Good	Low	Small
Bicone	Wide	Good	High	Large
TEM horn	Wide	Good	High	Large

The desire for high radiation efficiency is self-evident, but several types of broadband antennas employ resistive loading, which reduces efficiency. Other UWB antenna concerns include polarization properties (versus frequency), physical size, cost, and feeding techniques (balanced versus unbalanced). Table 2 summarizes several of these key features for a number of antennas that might be considered for UWB systems.

3.1.1. Transfer function for the radiated field from a UWB antenna

Consider the canonical UWB radio configuration shown in Figure 3, where the transmit antenna is driven with a voltage source $V_G(\omega)$ having an internal impedance $Z_G(\omega)$, and the receive antenna is terminated with load impedance $Z_L(\omega)$, with terminal voltage $V_L(\omega)$. The input impedances of the transmit and receive antennas are $Z_T(\omega)$ and $Z_R(\omega)$, respectively. The antennas are separated by a distance r, assumed to be large enough so that each antenna is in the far-field region of the other over the operating bandwidth.

We can define a frequency-domain transfer function that relates the radiated electric field $\vec{E}(\omega, r, \theta, \phi)$ to the transmit antenna generator voltage as

$$\vec{E}(\omega, r, \theta, \phi) = \vec{F}_{EG}(\omega, r, \theta, \phi) V_G(\omega), \tag{7}$$

where r, θ, ϕ are polar coordinates with origin at the transmitting antenna. For most antennas, the transfer function,

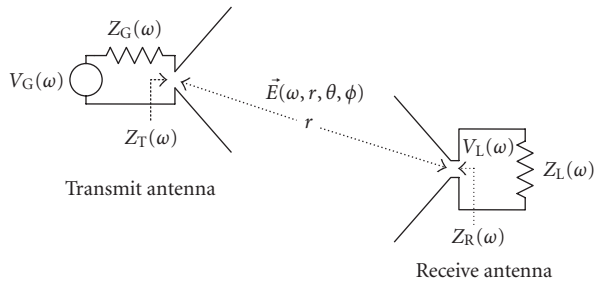

Figure 3: Frequency-domain model of transmit and receive antennas for a UWB radio system.

$\vec{F}_{EG}(\omega, r, \theta, \phi)$, must be calculated via numerical electromagnetic techniques (e.g., the moment method or finite-difference technique), as described in [21, 22, 23]. For the simple case of an electrically short dipole located on the z-axis, however, the result can be expressed in a closed form:

$$\vec{F}_{EG}(\omega, r, \theta, \phi) = \hat{\theta} \cdot \frac{j\omega\mu_0 h}{4\pi r} \cdot \frac{\sin\theta}{Z_G(\omega) + Z_T(\omega)} \cdot e^{-j\omega r/c}, \quad (8)$$

where h is the half length of the dipole, μ_0 is the permeability of free space, and c is the speed of light. This result shows that the radiated electric field is related to the derivative of the dipole current, but may be a more complicated function of the generator voltage, depending on the particular generator impedance and dipole input impedance functions.

Figure 4 shows the radiated electric field waveforms from several types of antennas, for a Gaussian monocycle generator waveform. Observe that the electrically short dipole provides good pulse fidelity, but at a relatively low amplitude. The resonant dipole provides a higher amplitude, and also greater duration. The log-periodic dipole array has very good impedance and gain bandwidth, but the nonconstant phase center causes considerable ringing of the radiated field. In contrast, the constant phase center of the Vivaldi antenna produces less ringing, and a very high amplitude pulse.

3.2. UWB link budget analysis

In this section we discuss the energy link loss between the transmitter and receiver of a UWB radio system. We assume here a baseband UWB system using short pulses; the link loss of a carrier-based multichannel UWB system can generally be well modeled using the traditional Friis equation. We first summarize the rigorous calculation of UWB energy transmission based on electromagnetic analysis of transient radiation and reception, including the effects of antenna impedance mismatches, pulse distortion effects, and the effects of frequency-dependent antenna gains and spreading factor. Next we present some closed-form approximations for energy link loss for the special cases of electrically small dipole antennas with Gaussian or Gaussian doublet (monocycle) generator waveforms. We also consider the application of the narrowband Friis transmission formula to a UWB radio system, and compare these results with the rigorous and approximate solutions for several types of antennas. This comparison shows that the use of the basic Friis formula can result in link loss errors of more than 60 dB for a UWB system with severely (impedance) mismatched antennas, but may give results correct to within a few dB for well-matched narrowband antennas, or by augmenting the formula with an impedance mismatch correction factor. We conclude that the dominant limitation of the Friis formula when applied to UWB systems is not the frequency dependence of the spreading factor or antenna gain terms, but the broadband effect of mismatch between the transmit/receive antennas and their source or load impedance. Pulse distortion effects also limit the accuracy of the Friis approximation, but to a much lesser degree.

3.2.1. Link loss based on rigorous electromagnetic analysis

The calculation of UWB energy link loss in the general case requires a complete transient electromagnetic solution for the transmit and receive antennas to account for the effects of impedance mismatch over the operating bandwidth, pulse distortion effects, and the effects of frequency-dependent antenna gains and spreading factor [18, 21, 22, 23]. With reference to Figure 3, define $H_{LG}(\omega)$ as the voltage transfer function that relates the receive antenna load voltage to the generator voltage at the transmit antenna [23, 24]:

$$V_L(\omega) = H_{LG}(\omega) V_G(\omega) e^{-j\omega r/c}, \quad (9)$$

where c is the speed of light. Note that the exponential factor representing the time delay between the transmit and receive antenna has been separated from the transfer function. Although not explicitly shown, it should be understood that this transfer function is dependent on the load impedance, the range between the antennas, and the elevation and azimuth angles at each antenna.

The time-domain voltage waveform at the receive antenna can be found as

$$v_L(t') = \frac{1}{2\pi} \int_{BW} H_{LG}(\omega) V_G(\omega) e^{j\omega t'} d\omega, \quad (10)$$

where $t' = t - r/c$ is the retarded time variable.

The energy delivered to the transmit antenna by the source is given by

$$W_{in} = \frac{1}{2\pi} \int_{BW} \frac{|V_G(\omega)|^2 R_T(\omega)}{|Z_T(\omega) + Z_G(\omega)|^2} d\omega, \quad (11)$$

where $R_T(\omega)$ is the real part of $Z_T(\omega)$. The energy received by the load at the receive antenna is given by

$$W_{rec} = \frac{1}{2\pi} \int_{BW} \frac{|V_L(\omega)|^2}{Z_L^*(\omega)} d\omega. \quad (12)$$

The integrations in (10)–(12) are over the bandwidth of the generator waveform.

To calculate energy link loss for a specific set of antennas and a given generator waveform, the transfer function of

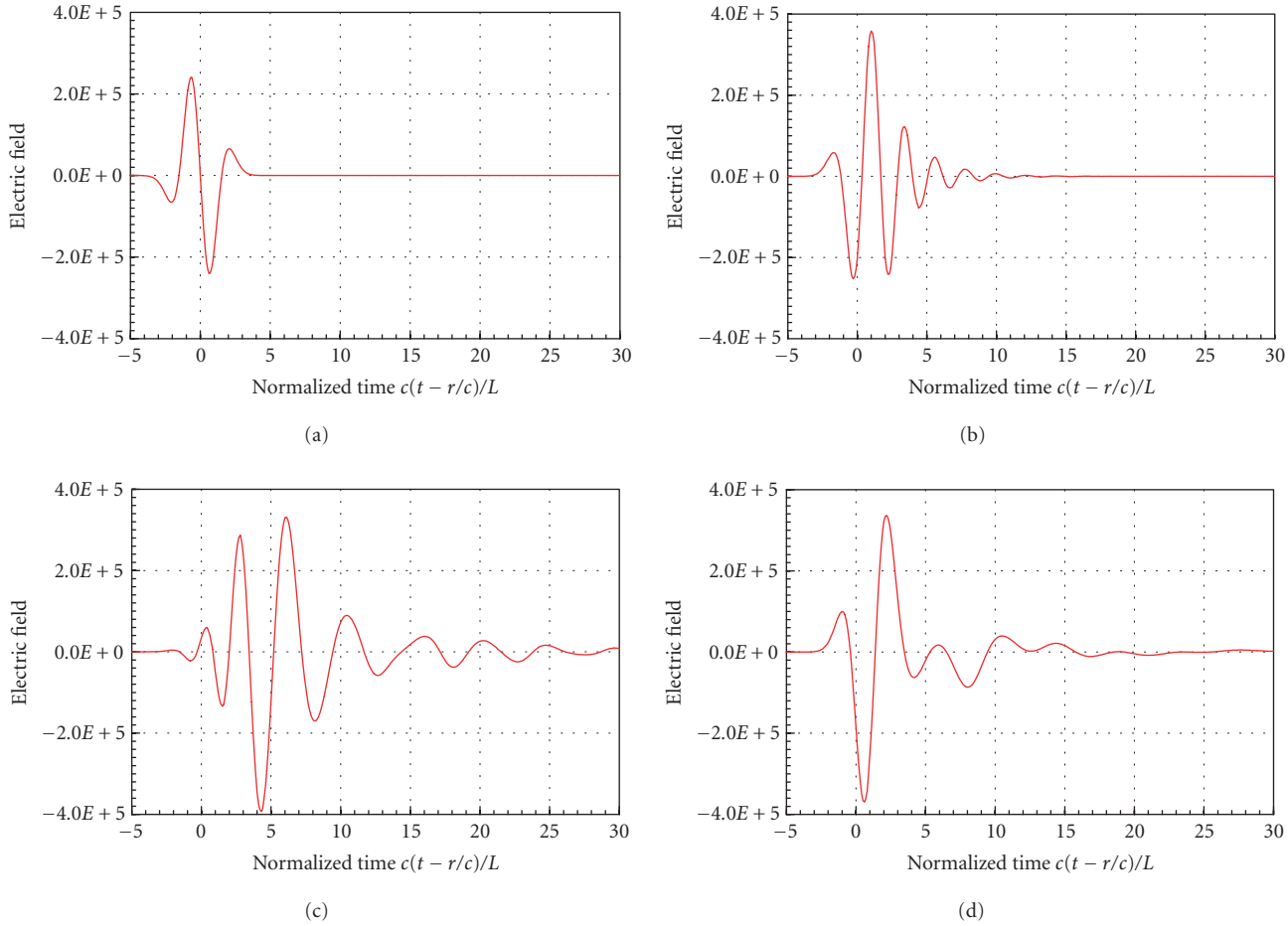

FIGURE 4: Radiated electric field waveforms for antennas with a Gaussian monocycle generator waveform ($T = 4.42 \times 10^{-10}$ seconds). The field is normalized by the factor $re^{j\omega r/c}$. (a) Short dipole ($L = 1.0$ cm), (b) resonant dipole ($L = 15$ cm), (c) log-periodic dipole array, and (d) Vivaldi antenna.

(9) is first computed over a range of frequencies that cover the system bandwidth (as determined by the spectrum of the generator waveform). This can be done using a numerical electromagnetic analysis techniques. Then the input and received energies can be computed using (11) and (12). The link loss is defined as the ratio of these two quantities. Note that this calculation includes polarization mismatch, propagation losses, antenna efficiency, impedance mismatches, and waveform distortion effects.

For the results that follow, we define a Gaussian generator waveform as

$$v_G(t) = V_o e^{-t^2/2T^2} \tag{13}$$

and a monocycle (Gaussian doublet) generator waveform as

$$v_G(t) = V_o \frac{t}{T} e^{-t^2/2T^2}. \tag{14}$$

Note that the Gaussian pulse has nonzero DC content, although this does not contribute to either the input energy W_{in} or received energy W_{rec} for realistic antennas.

3.2.2. Closed-form approximations for UWB link loss for short dipole

Using reasonable approximations, it is possible to derive closed-form expressions for the energy link loss of a UWB radio system using electrically small dipoles or loops, and either a Gaussian pulse or a monocycle generator waveform [24]. These results appear to be the only cases that can be expressed in closed form and are therefore useful for showing the dependence of waveform shape, receiver impedance, and gain factors in more general situations. Additionally, the accessibility of these results should be useful for systems engineers working with UWB radio technology.

In the following results, we assume that both transmit and receive antennas are identical, are polarization matched, and are oriented so that each is in the main beam of the other. For electrically short lossless dipoles of half length $h = L/2$ and radius a, the energy link loss can be expressed for Gaussian and monocycle input waveforms, for either small or large values of load resistance, R_L, as shown in Table 3. In the above results, $C_o = -h/120c[1 + \ln(a/h)]$ is the capacitance of the dipole, c is the speed of light, and $\eta_o = 377\,\Omega$ is the

Table 3: Closed-form approximations for UWB link loss for short dipoles.

Input waveform	Link loss for small R_L	Link loss for large R_L
Gaussian pulse	$\frac{W_{rec}}{W_{in}} = \frac{15\eta_o R_L}{16\pi}\left(\frac{C_o h}{Tr}\right)^2$	$\frac{W_{rec}}{W_{in}} = \frac{3\eta_o h^2}{8\pi r^2 R_L}$
Monocycle	$\frac{W_{rec}}{W_{in}} = \frac{21\eta_o R_L}{16\pi}\left(\frac{C_o h}{Tr}\right)^2$	$\frac{W_{rec}}{W_{in}} = \frac{3\eta_o h^2}{8\pi r^2 R_L}$

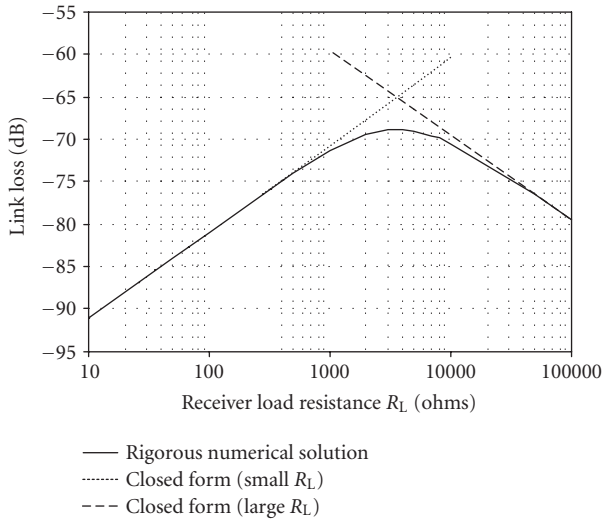

Figure 5: Comparison of closed form versus exact (numerical) energy link loss (multiplied by r^2) for a UWB system using two electrically short dipoles and a monocycle generator waveform versus receive load resistance. Dipole length = 1.0 cm, dipole radius = 0.02 cm, $Z_G = 50\,\Omega$, and $T = 4.42 \times 10^{-10}$ seconds.

impedance of free space. These approximations are accurate for frequencies up to where the dipole length is less than $\lambda/20$. Over this range, the input resistance is less than 0.5 Ω, while the input reactance is at least several thousand ohms.

Figure 5 shows a comparison of the closed-form energy link loss results from Table 3 compared with rigorous data from a moment method solution for a short dipole, versus load resistance, for the monocycle generator waveform. For these parameters, it is seen that the "small R_L" result works well for R_L up to about 1000 Ω, while the "large R_L" form works well down to about 20 000 Ω. Optimum link loss is seen to occur between these values.

3.2.3. Link loss using the narrowband Friis transmission formula

The Friis link equation that applies to narrowband (carrier-based) radio systems is given by [25]

$$P_r(\omega) = P_t(\omega)\frac{G_t(\omega)G_r(\omega)\lambda^2}{(4\pi r)^2}, \tag{15}$$

where $P_r(\omega)$ and $P_t(\omega)$ are the received and transmitted powers at operating frequency ω rad/s, $G_t(\omega)$ and $G_r(\omega)$ are the transmit and receive antenna power gains, respectively, and λ is the wavelength at the operating frequency. Note that this result does not include propagation losses, polarization mismatch, or impedance mismatch at either the transmit or receive antenna. Also, the Friis formula, since it applies only to the power in CW (sinusoidal) signals, does not account for pulse distortion effects at either antenna or even the type of waveform used at the generator.

If the transmitted signal consists of digital data at a bit rate R_b bps, then the energies per bit on transmit and receive are $E_{bt} = P_t/R_b$ and $E_{br} = P_r/R_b$, respectively. Then (15) can be written in terms of the transmit and receive bit energy densities as

$$E_{br}(\omega) = E_{bt}(\omega)\frac{G_t(\omega)G_r(\omega)\lambda^2}{(4\pi r)^2}. \tag{16}$$

The frequency dependence of each term is explicitly shown in (15) and (16). Note that the spread factor $(r/\lambda)^2$ has a frequency dependence of 6 dB per octave, but this is reduced to a maximum error of 3 dB at either end of an octave bandwidth for a single frequency chosen at midband. Similarly, the frequency variation of antenna gain is typically small over a wide frequency range for many practical antenna elements. An electrically short dipole antenna, for example, has a gain of about 1.8 dB for all frequencies below resonance. The effect of impedance mismatch can be included (at a particular frequency ω) by multiplying (16) by the factor $(1 - |\Gamma(\omega)|^2)$, where $\Gamma(\omega)$ is the reflection coefficient at the receive antenna given by

$$\Gamma(\omega) = \frac{Z_R - Z_L}{Z_R + Z_L}. \tag{17}$$

Note that the effect of mismatch at the generator is not included—this is because we have chosen to use W_{in}, the energy delivered to the transmit antenna, as opposed to the energy available from the generator.

3.2.4. Examples and comments

To compare specific numerical results, we consider the link loss for three different transmit/receive antenna pairs, with Gaussian and monocycle waveforms. Choosing $T = 4.42 \times 10^{-10}$ seconds for both the Gaussian pulse and the monocycle waveforms results in a 10 dB bandwidth of 550 MHz for the Gaussian pulse, and a 10 dB bandwidth of 70 MHz to 790 MHz for the monocycle pulse. The Gaussian waveform contains power at very low frequencies (and DC), which is not radiated by any of the antennas considered here. The parameters for each of the three antennas are given below.

An electrically short dipole

Dipole length = 1.0 cm, dipole radius = 0.02 cm, and $Z_L = Z_G = 50\,\Omega$. The 10 dB bandwidth for the magnitude of the resulting transfer function is from 10.2 GHz to 18.9 GHz. This element is severely mismatched over the bandwidth of either input signal.

Table 4: Normalized ($r = 1$) energy link loss for various antennas and excitations.

Antenna	Gaussian rigorous ((9)–(12), (13))	Monocycle rigorous ((9)–(12), (14))	Midband frequency	Midband Friis ((16))	Midband Friis and Z-mismatch
Short dipoles	−85.5 dB	−84.0 dB	430 MHz	−20.8 dB	−87.0 dB
Resonant dipoles	−23.9 dB	−23.9 dB	500 MHz	−22.1 dB	−22.4 dB
Lossy dipoles	−43.1 dB	−41.8 dB	500 MHz	−22.1 dB	−22.3 dB

A resonant dipole

Dipole length = 30.0 cm, dipole radius = 0.02 cm, and $Z_L = Z_G = 72\,\Omega$. The 10 dB bandwidth for the magnitude of the resulting transfer function is from 410 MHz to 580 MHz. This is a relatively narrowband element, but is well matched to the source and load impedances at its resonant frequency of 500 MHz.

A lossy resonant dipole

Dipole length = 30.0 cm, dipole radius = 0.02 cm, dipole conductivity = 100 S/m, and $Z_L = Z_G = 800\,\Omega$. The 10 dB bandwidth for the magnitude of the resulting transfer function is 190 MHz to 990 MHz. This is a broadband element, and is reasonably well matched to the source and load impedances over the bandwidth of the input signals. Due to the lossy loading, the efficiency of this element is about 10%.

The resulting energy link losses for these antennas are shown in Table 4. The first two columns of data refer to the rigorous calculation of link loss using a full electromagnetic solution summarized by (9)–(12) for the Gaussian and monocycle input pulses. These solutions include all relevant effects, including impedance mismatch, pulse distortion, and frequency variation of gain and propagation factors. Observe that the link loss differs by a few dB for the two different input pulses when broadband elements are used (short dipoles or lossy dipoles). In contrast, waveform shape has little effect on link loss when the antennas are relatively narrowband (resonant dipoles), since the relatively narrow portion of the input spectrum that is passed by the antennas results in an essentially sinusoidal waveform.

The remaining three columns present data associated with the Friis formula of (16). The midband frequency is the frequency at which the calculation is performed, and has been selected to be at the maximum response of the associated transfer function (for the resonant and lossy dipoles), or near the midband of the input waveform bandwidth (for the short dipoles). The gain for each antenna was assumed to be constant at 1.8 dB. Note that using the basic Friis formula without impedance mismatch correction gives an error of more than 60 dB when the antennas are severely mismatched (short dipoles) but gives results within a few dB of the correct result for narrowband matched antennas (the resonant dipoles). If the efficiency of the lossy dipoles is included in the Friis calculation (10% efficiency, or 20 dB loss for combined transmit and receive antennas), reasonable results (−42.3 dB) are also obtained for this case.

We conclude that for narrowband antennas, the Friis formula can give results within about 1 dB for UWB systems (of course, it is generally undesirable to use such narrowband antennas for a wideband system). For broadband elements, application of the Friis formula with the impedance mismatch factor can produce results that are accurate to about 3 dB. More complicated elements, such as arrays or traveling wave antennas, will likely lead to different conclusions.

In a general sense, the essential problem with short-pulse radio transmission that differentiates it from a narrowband (CW) system is the distortion introduced by practical transmit and receive antennas. These antennas, which form the interface between plane waves and circuitry at both the transmitter and receiver, are a direct cause of pulse distortion in a UWB radio system. Fundamentally, this is due to non-TEM (reactive) fields in the near zone of each antenna, which lead to the impedance mismatch terms noted above as well as the radiation mechanism itself. In principle, it is possible to use pure TEM mode antennas (e.g., infinite biconical and TEM horns) to achieve distortionless pulse transmission and reception, but this is of limited practicality because of the large sizes required for such antennas to avoid end reflections.

Finally, we note that the fact that the overall energy link loss in a UWB system depends on generator pulse shape implies that it is possible to optimize receive pulse amplitude or energy by proper generator waveform selection. Such optimal waveforms can be derived for a specific set of transmit and receive antennas, and can result in an improvement of several dB over the results obtained with Gaussian or Gaussian monocycle waveforms [23]. Although it is generally not practical to implement a UWB system with these optimal waveforms, such results are useful because they set an upper limit on the performance of the system.

3.3. UWB propagation

In principle, one technique for evaluating a UWB channel is to drive the transmitting antenna with a short pulse and record the response on a digital oscilloscope (see the UltRa Lab website). We can illustrate this in Figure 6 with a set of measurements made in several different environments with the same pulse generator and antennas. Notice first that the transmitted waveform in Figure 6a is a short pulse on the order of a half nanosecond in duration, so these illustrative measurements are just below the FCC approved communications band. The measurements that we have made outdoors tend to be relatively free of dense multipath, partly because the low-power nature of the signal precluded observable reflections from distant objects. One such measurement,

shown in Figure 6b, displays the direct path response to the transmitted pulse in the first four (approximately) nanoseconds of the response function, indicating the filtering effect that the antenna system has on the transmitted signal.

Indoor communications (see Figures 6c and 6d) clearly demonstrates dense diffuse multipath effects with decay time constants of the response envelope being on the order of 50 to 100 nanoseconds in an office/lab building. In the extreme environment of the empty hold of a cargo ship (Figures 6e and 6f), the decay time constants exceeded one microsecond, indicating extreme RF echoing in the metallic hold of the ship. These shipboard measurements were made over longer distances than the other measurements and are somewhat noisy (see http://ultra.usc.edu/new_site/experiments.html). When there is an unobstructed line of sight (LOS) between the transmitting and receiving antenna (e.g., see Figures 6c and 6e), the initial part of the response function, corresponding to the direct propagation path, is usually the largest in amplitude, making the direct path response readily identifiable for accurate ranging purposes. In situations in which the direct path is blocked by objects that may reduce or eliminate the direct path signal, there is usually an initial growth to the response envelope before a decay, as illustrated in Figures 6d and 6f.

Statistical models for UWB propagation [26, 27, 28, 29] have been developed for indoor channels, and UWB measurement databases currently are available over the internet (see http://ultra.usc.edu/new_site/database.html). The IEEE 802.15.3a standardization group, charged with developing a UWB standard for personal area networks, has developed four UWB indoor channel models to support its evaluation of proposed UWB signaling standards. The development of these models and the details of their structure are described in [30]. These models are quite similar to the cluster models of Saleh and Valenzuela [31].

The analysis of arrays of measurements in [26] used a version of the CLEAN algorithm to determine the angles of arrival, as well as propagation delay and amplitude, for each signal component. With the addition of the angle parameter, it is possible to break up the collection of signal components into disjoint groups (clusters) sharing similar angles of arrival and propagation delays. The earliest signal component in a cluster (the cluster leader) serves as a reference from which to measure the relative angle of arrival, amplitude, and delay of other cluster components. One can presume that the components in the cluster followed roughly the same path to the receiver, and that the gross properties of the path (major attenuation, e.g., caused by walls, and delay components) are captured by the attenuation and delay of the cluster leader. Deviations of other cluster components parameters from those of the cluster leader are quite regular, with angle deviation having a truncated two-sided Laplacian distribution [26, 32], and relative amplitude being roughly Rayleigh, the latter choice of distribution being as much for simplicity as accuracy. It is also worth noting here that while the signal with unobstructed propagation path from the transmitter to the receiver may be referred to as the direct-path signal, it is often difficult to determine if two signal components that are close in time and angle are caused by distinct propagation effects (i.e., distinct propagation paths) or are caused by filtering effects that occur during reflections from a given object or transmission through a given object. Hence, the word path must be used with care in referring to signal decompositions.

Most of the indoor channel measurement work of which we are aware has been performed with identically polarized antennas. It should be noted here that cross-polarization effects are not included in these models, and more generally, there is no reliable way to substitute one antenna type or orientation for another and expect to accurately predict, in detail, the effect of the exchange from the original indoor channel measurement.

4. UWB CIRCUIT AND ARCHITECTURE CHALLENGES

Although great headway has recently been made in efficient implementation of narrowband radios, the UWB signal has fundamentally different signal characteristics, making existing receiver circuits and architectures ill-suited for UWB use. The signal bandwidths and fractional bandwidths of UWB radio are at least an order of magnitude greater than those of existing narrowband radios. Furthermore, the UWB radio must coexist with many other narrowband systems transmitting and receiving in the same bandwidth. Consequently, a UWB radio must have intrinsically different sensitivity, selectivity, and bandwidth requirements, which motivate radio circuit and architectural designs that are substantially different from their narrowband counterparts.

In a UWB receiver, the analog-to-digital converter (ADC) can be moved almost up to the antenna, resulting in a dramatic reduction of the required analog circuitries, which often dominate the size, power, and cost of a modern receiver. A block diagram of the UWB receiver is shown in Figure 7. Critical to this design approach, however, is the ability for the ADC to efficiently sample and digitize at least at the signal Nyquist rate of several GHz. The ADC must also support a very large dynamic range to resolve the signal from the strong narrowband interferers. Currently, such ADCs are far from being practical.

The bandwidth and dynamic range requirements of the UWB radio appear to have led to two alternative development paths. In the first, the UWB system is scaled down to operate at a greatly reduced bandwidth, compromising the benefits of the UWB radio. An example of such a system is the time-frequency interleaved (TFI) OFDM radio proposed as a possible candidate for the 802.15 WPAN standard [33]. In the other development path, receiver functions such as correlation are performed in the analog domain before digitizing at a much reduced sampling frequency. Such analog receivers are less flexible and suffer from circuit mismatches and other nonidealities. These circuit nonidealities limit the number of analog correlators that can be practically realized on an integrated circuit (IC). Since many correlators are required to exploit the diversity available in a UWB system,

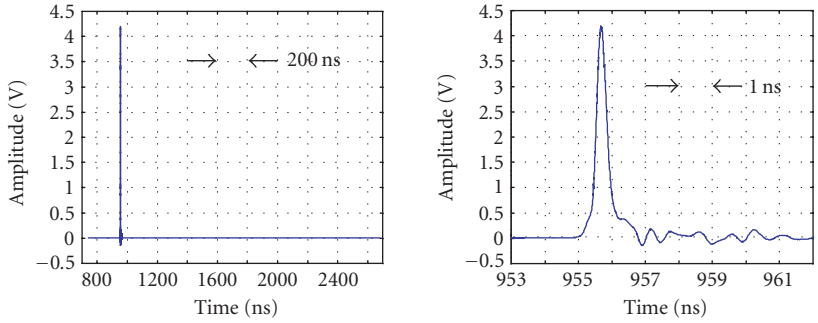

(a) Pulse driving transmitting antenna.

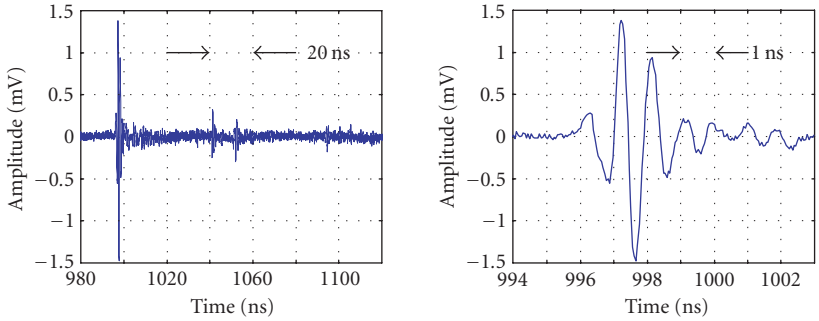

(b) Typical outdoor received signal.

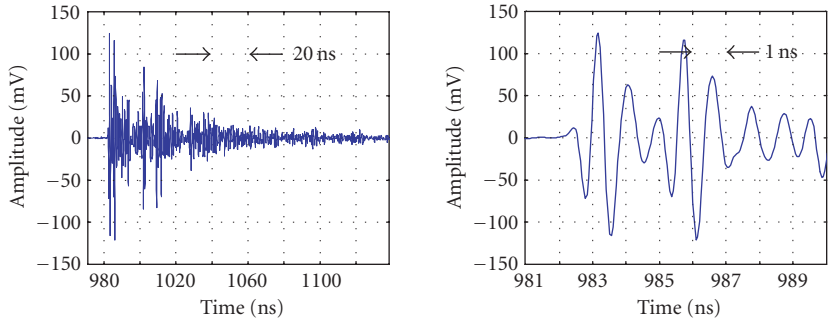

(c) Typical indoor received signal, clear line-of-sight.

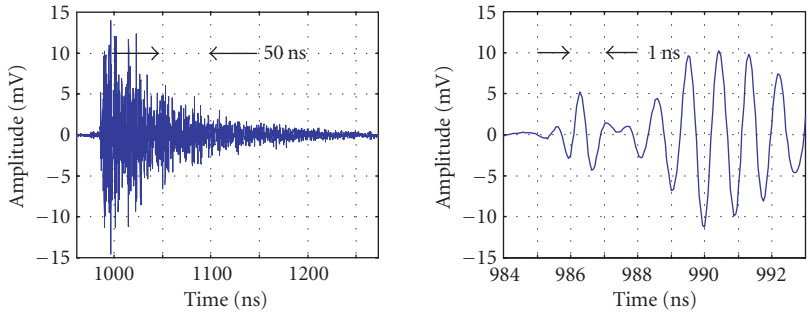

(d) Typical indoor received signal, blocked line-of-sight.

Figure 6: Transmitted signal and typical received signal waveforms in five different environments. The received signal in each environment is shown in two different time scales: the left plot encompasses the response decay time, and the right plot is set at one nanosecond per division to show the leading edge of the response.

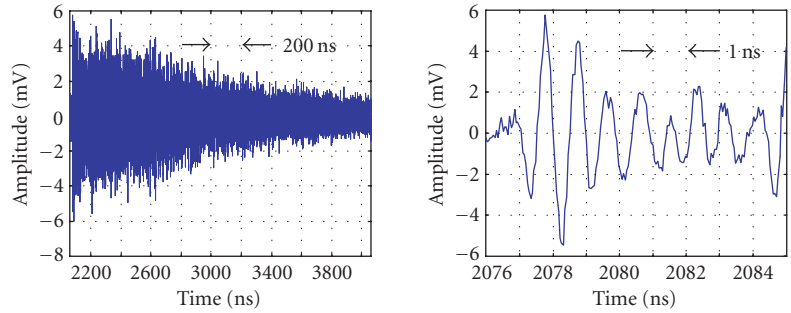

(e) Cargo-hold received signal, clear line-of-sight.

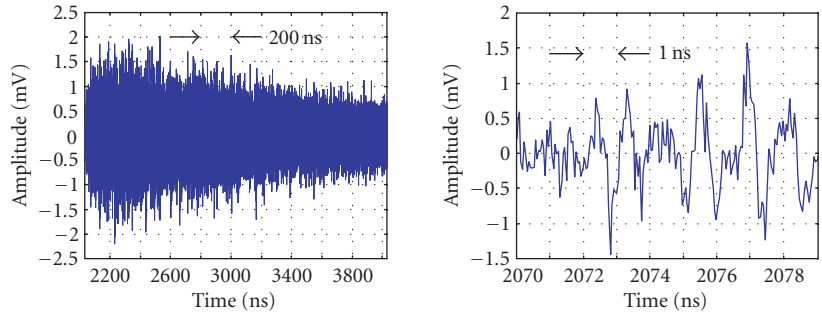

(f) Cargo-hold received signal, blocked line-of-sight.

Figure 6: Continued.

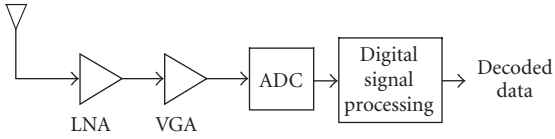

Figure 7: Block diagram of a UWB receiver.

analog receivers generally do not perform well. These circuit nonidealities also preclude the use of sophisticated narrowband interference suppression techniques, which can greatly improve the receiver performance in environments with large narrowband interferers such as in UWB systems. To achieve high reception performance, therefore, the UWB signal needs to be digitized at the signal Nyquist rate of several GHz, so that all of the receiver functions are performed digitally. In addition, as digital circuits become faster and denser with constant scaling of CMOS technology, simplifying the analog circuits as much as possible and distributing as much of the analog operations to the digital domain should prove more beneficial.

There are numerous implementation challenges in the UWB radio. Chief among them are the extremely high-sampling ADC and the wideband amplification requirements, both of which are described in the following sections. Other design challenges include the generation of narrow pulses at the transmitter and digital processing of the received signals at high clock frequencies.

4.1. Digital receiver architectures

Since designing a single ADC to operate at the signal Nyquist rate is not practical, parallel ADC architectures with each ADC operating at a fraction of the effective sampling frequency need to be employed. To sample at a fraction of the effective sampling frequency, the received UWB signal can be channelized either in the time or frequency domain. An approach that has been used in high-speed digital sampling oscilloscopes is to employ an array of M ADCs each triggered successively at $1/M\times$ the effective sample rate of the parallel ADC. A fundamental problem with an actual implementation of such time-interleaved architecture is that each ADC sees the full bandwidth of the input signal. This causes great difficulty in the design of the sample/hold circuitry. Furthermore, in the presence of strong narrowband interferers, each ADC requires an impractically large dynamic range to resolve the signal from the narrowband interferers.

Instead of channelizing by time-interleaving, the received signal can be channelized into multiple frequency subbands with an ADC in each subband channel operating at a fraction of the effective sampling frequency. The received UWB signal is split into M subband signals using M analysis filters. The resulting signals are sampled at f_{eff}/M, where f_{eff} is the effective sampling frequency of the receiver, and digitized using M ADCs. Based on the frequency-channelized signals, the receiver performs all of the receiver functions including narrowband interference suppression and cancellation of aliasing from sampling.

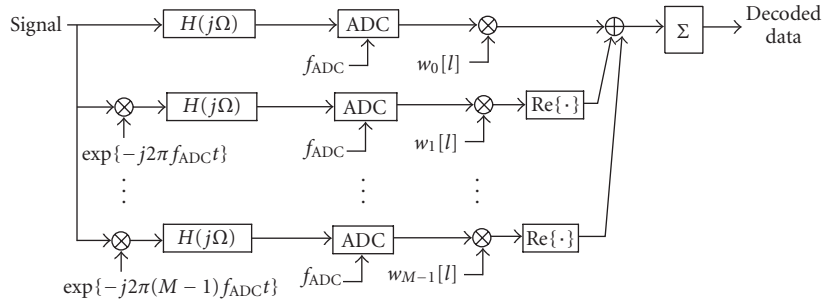

Figure 8: Block diagram of a frequency-channelized UWB receiver.

An important advantage of channelizing in the frequency domain, instead of in the time domain, is that the dynamic range requirement of each ADC is relaxed, since the frequency-channelization process isolates the effects of large narrowband interferers. The sample/hold circuitry, however, is still very difficult to design as it sees the uppermost frequency in the high-frequency subband channels. In addition, sharp bandpass filters with high center frequencies, which are necessary to mitigate the effects of strong narrowband interferers, are extremely difficult to realize, especially in ICs.

Instead of using bandpass filters with high center frequencies, channelization can be achieved using a bank of M mixers operating at equally spaced frequencies and M lowpass filters to decompose the analog input signal into M subbands. The lowpass channelization can also be achieved by cascading a bank of mixers and lowpass filters. A block diagram of a frequency-channelized receiver is shown in Figure 8. A total of $2M-1$ ADCs, each operating at f_{ADC}, is employed to achieve an effective sampling frequency of $(2M-1)f_{ADC}$. In addition to obviating the need to design high frequency bandpass filters, channelizing the received signal using this approach greatly relaxes the design requirements of the sample/hold circuitry. The sample/hold circuitry in this lowpass channelized architecture sees only the bandwidth of the subband signal; whereas in the bandpass channelization approach, the sample/hold circuitry sees the uppermost frequency in the high-frequency subbands.

When no narrowband interferers are present, the performance of the time-interleaved and frequency-channelized receivers are nearly identical. However, when finite resolution ADCs are employed in the presence of large narrowband interferers, the frequency-channelized receiver significantly outperforms the time-interleaved receiver. This effect is illustrated in Figure 9, which plots the SNR after correlation of a single pulse versus the filter order of the lowpass filter $H(j\Omega)$. The frequency-channelized and time-interleaved receivers each employ nine ADCs. The narrowband interferer centered at the peak of the signal spectrum is assumed to have a bandwidth of 15% of the signal bandwidth and magnitude of 50 dB greater than the white noise floor. When infinite bit resolution is available, the filter order does not affect the receiver performance. However, when there are only a finite number of bits in the ADC, the performance of the frequency-channelized receiver improves steadily compared to the time-interleaved receiver as the filter order increases.

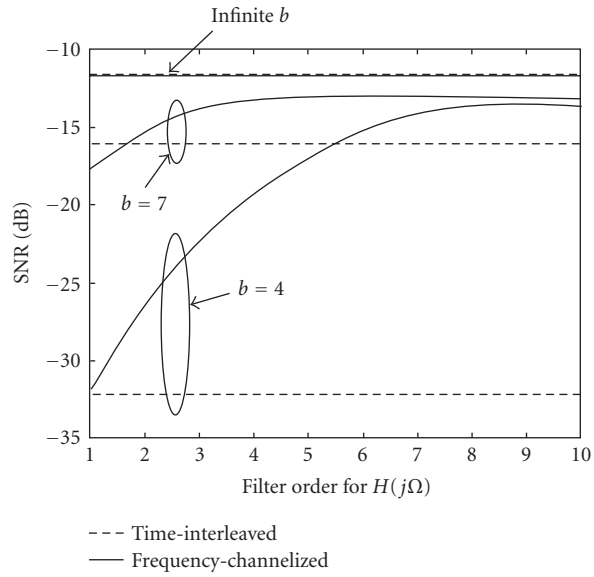

Figure 9: SNR versus lowpass filter order.

This improvement saturates when the filter order is approximately four for 7 bits and eight for 4 bits, which correspond to performance improvements of roughly 7 dB and 20 dB, respectively, compared to the time-interleaved receiver.

This large performance difference arises for sharper filters because the frequency-channelization process better isolates the effects of the narrowband interferer by raising the quantization noise floor mostly in the subband channels containing the interferers. Since significant interference noise is already present in these subband channels, the additional quantization noise does not greatly increase the total noise power relative to the signal power. By contrast, a narrowband interferer in the time-interleaved receiver increases the quantization noise floor across the entire signal spectrum. Thus, even in frequencies with no interference, the quantization noise floor is significantly raised relative to the signal power, resulting in large overall performance degradation. The ability to isolate the narrowband interferer significantly improves the performance of the frequency-channelized receiver compared to the time-interleaved receiver, especially when low resolution ADCs are employed for complexity reasons [34].

The frequency-channelized receiver requires accurate knowledge of the transfer functions of the analog filters. Since exact knowledge is not available in practice due to fabrication process and temperature variations, adaptive techniques are needed. An adaptive frequency-channelized receiver, however, suffers from poor convergence speed compared to an ideal full band receiver because of the increased number of parameters to estimate and the slow convergence rates of the adaptive cross-filters that eliminate subband aliasing. This poor convergence speed can be problematic in time-varying wireless systems such as in UWB. In several UWB systems, however, the frequency-channelized receiver can be made to achieve convergence speeds comparable to a full band receiver. Examples of such systems are described in [35, 36, 37].

4.2. Wideband amplification

The performance of an amplifier is generally quantified using the noise factor (or noise figure (NF) in dB), which is defined as the ratio of the signal-to-noise ratio (SNR) at the input of the amplifier to the SNR at the output of the amplifier. Although the use of the NF metric is straightforward in narrowband systems, its use becomes more difficult in UWB systems. The main difficulty arises in defining the SNR. In a narrowband system, where both the input signal and noise are assumed to be a single tone at the carrier frequency, the SNR is obtained by simply dividing the signal power by the noise power. In a UWB system, however, the input signal is broadband and the additive noise may be colored. The SNR obtained by simply dividing the signal power by the total noise power (whose bandwidth must also be defined) is less meaningful, since a higher SNR value defined in this manner does not necessarily translate to a higher receiver performance. This is because the performance of the receiver after the digital decoding process does not depend on the total signal and noise power but on the PSD of the additive noise and the impulse responses of the propagation channel and the transmit pulse. Because of the difficulty in defining the SNR, existing work on broadband amplifiers defines the NF as the weighted average of the single-tone NF (or spot NF). Although such definition of NF is an extension of a single-tone NF, minimizing such arbitrary performance metric does not necessarily improve the overall receiver performance.

For the NF of the amplifier to be a meaningful metric in a UWB receiver, the SNR at the input and output of the amplifier should measure the achievable performance after the eventual digital decoding process because it is ultimately the most relevant measure of performance. Hence, the SNR is defined as the matched-filter bound (MFB), which represents an upper limit on the performance of data transmission systems. The MFB is obtained when a noise whitened matched filter is employed to receive a single transmitted pulse. By defining the SNR as the MFB, the NF measures the degree of degradation in the achievable receiver performance caused by the amplifier. This NF is referred to as the effective NF. The effective NF can be shown to be the weighted harmonic mean of the single-tone NF, where the weights are proportional to the signal spectral density [38].

The amplifier that sets the NF of the overall receiver is the low-noise amplifier (LNA), which is the first amplifier in the receive chain. Since the LNA interfaces with the external world, an additional constraint on the input impedance is typically placed on the LNA. Designing the LNA to minimize the effective NF while satisfying the input impedance requirement across the entire frequency band of interest is in general difficult, especially when CMOS technology with on-chip passive components is employed to achieve high levels of integration and lower cost. Most of the existing work on CMOS-LNA has concentrated on optimizing at a single frequency, which is accurate and yield good performance in narrowband communication systems. For a UWB system, however, the UWB nature of the signal clearly invalidates the single-frequency assumption. Existing CMOS-LNA design techniques therefore must be extended to efficiently support a wideband source. Recently, several wideband CMOS-LNA designs have been proposed [39, 40].

5. UWB SYSTEM CHALLENGES

5.1. Modulation design: efficiently staying within the FCC limits

One of the challenges of UWB signal design is to get the maximum signal power to the receiver, while satisfying the FCC mask on the EIRP of the UWB signal. The structure of this problem is illustrated here. We define the impulse response from source voltage $v_G(t)$ to the far electric field $\vec{e}(t, r, \theta, \phi)$ in direction ϕ, θ at range r to be $\vec{h}_{EG}(t)$ (with Fourier transform $\vec{H}_{EG}(f)$). The Fourier transform of the electric field vector is

$$\begin{aligned}\vec{E}(2\pi f, r, \theta, \phi) &= \int_{-\infty}^{\infty} \vec{e}(t, r, \theta, \phi) e^{-j2\pi f t} dt \\ &= \vec{H}_{EG}(f) V_G(f) \quad \text{volts/meter-Hertz.}\end{aligned} \tag{18}$$

The energy density per unit wavefront area per Hertz at the point (r, θ, ϕ) is $|\vec{E}(2\pi f, r, \theta, \phi)|^2/\eta$ joules per square-meter-Hertz, where $\eta = 377\,\Omega$. The effective isotropic radiated energy density of this signal is equal to

$$\begin{aligned}&\frac{2\pi r^2 \left|\vec{E}(2\pi f, r, \theta, \phi)\right|^2}{\eta} \\ &\quad = \frac{2\pi r^2}{\eta} \cdot \left|\vec{H}_{EG}(f)\right|^2 \cdot \left|V_G(f)\right|^2.\end{aligned} \tag{19}$$

If instead the source voltage $v_G(t)$ is a finite power signal with PSD $S_G(f)$ volts^2 per Hertz, then effective isotropic radiated power density equals

$$\frac{2\pi r^2}{\eta} \cdot \left|\vec{H}_{EG}(f)\right|^2 \cdot S_G(f). \tag{20}$$

The FCC regulation states that the EIRP measured in dBm in every 1 MHz bandwidth must be less than a bounding mask $M(f)$. Hence, a reasonable model for satisfying this

requirement is that

$$10\log_{10}\left(\frac{2\pi r^2}{\eta}\int_{f_o-0.5\times10^6}^{f_o+0.5\times10^6}\left|\vec{H}_{EG}(f)\right|^2\cdot S_G(f)df\right)+30 < M(f_o)\quad \text{dBm}. \tag{21}$$

Suppose that the transmitter can signal with a set of D UWB source voltage waveforms $v_{Gd}(t)$, $d = 1,\ldots,D$, each of the form

$$v_{Gd}(t)=\sum_{j=1}^{N_p}a_j^{(d)}p_G\left(t-\tau_j^{(d)}\right)=\underbrace{\left(\sum_{j=1}^{N_p}a_j^{(d)}\delta_D\left(t-\tau_j^{(d)}\right)\right)}_{\triangleq\delta^{(d)}(t)}\star p_G(t). \tag{22}$$

Here $\delta_D(t)$ represents a Dirac delta function and $\star$ represents convolution, so that $\delta^{(d)}(t)$ can be viewed as the impulse response function of pattern generator d. We will use $\Delta^{(d)}(f)$ to represent the system function of the dth pattern generator, that is, the Fourier transform of $\delta^{(d)}(t)$:

$$\Delta^{(d)}(f)=\sum_{j=1}^{N_p}a_j^{(d)}e^{-j2\pi f\tau_j^{(d)}}. \tag{23}$$

This mathematical model for the source generator voltage can be adapted or generalized to represent many of the digital modulation formats contemplated for UWB use. If a signal $v_{G1}(t)$ is transfered repeatedly at a rate of one every T_p seconds to construct $v_G(t)$, then the resulting line PSD $S_G(f)$ is

$$S_G(f)=\frac{1}{T_p^2}\cdot\left|\Delta^{(1)}(f)\right|^2\cdot\left|P_G(f)\right|^2\times\sum_{n=-\infty}^{\infty}\delta_D\left(f-\frac{n}{T_p}\right)\quad\text{(periodic signal)}. \tag{24}$$

On the other hand, we assume that an infinite sequence of waveforms is selected independently and equally likely at random from a set of D possible waveforms of the form (22), and that this sequence is transmitted at the rate of one waveform every T_p seconds. Under the further assumption that the waveform set is efficiently designed, that is, $\sum_{d=1}^{D}v_{Gd}(t)=0$, the PSD $S_G(f)$ of the resulting signal is[2]

$$S_G(f)=\frac{1}{MT_p}\cdot\left|P_G(f)\right|^2\cdot\sum_{d=1}^{D}\left|\Delta^{(d)}(f)\right|^2\quad\text{(efficient data modulation)}. \tag{25}$$

It is worth noting that testing of a UWB transmission's regulatory compliance in both cases, that is, with data modulation switched on and with data modulation switched off, may be required.

Determining compliance of a design with the EIRP mask analytically requires separately substituting (24) and (25) into (21) and checking to see that the relation (21) is satisfied in the prescribed measurement environment for all choices of θ and ϕ. Hence, compliance is determined by the choices of the pulse shape's energy spectrum $|P_G(f)|^2$, the pattern generator's power transfer profile (either $|\Delta^{(1)}(f)|^2$ or $\sum_d|\Delta^{(d)}(f)|^2$), and the power transfer function $|\vec{H}_{EG}(f)|^2$ to the radiating electric far field.

5.1.1. Pulse-shape design

Within the above model for compliance, there are many possible approaches to modulation design. Typically shaping to fit the mask is accomplished by the design of the pulse shape $p_G(t)$ and the remaining physical structures that influence $\vec{h}_{EG}(t)$, for example, filters, antennas, and so forth. The major difficulty is that designing the shape of the electric field pulse $p_E(t)=p_G(t)\star h_{EG}(t)$ to have energy spectral density shaped to fit the mask does not generally yield a solution for the source pulse $P_G(f)=P_E(f)/\vec{H}_{EG}^{-1}(f)$ that is time limited.[3]

Figure 10a illustrates two transmitted signals, the continuous waveform efficiently filling a rectangular portion of the spectrum (solid trace of Figure 10b). The receiving antenna further shapes the spectral density, in this case attenuating the higher frequencies (dashed trace of Figure 10b). Arbitrary UWB waveforms can be approximated by digital-to-analog converters (DAC). Figure 10a also contains a 3-bit quantized approximation of the original continuous signal, which if transmitted, gives the energy spectra of Figure 10c. In this example, the DAC pulse generator causes an inefficient spectral ripple in the PSD of the far-field signal, which adds to the spectral distortion caused by the receiving antenna. Computations like those producing Figure 10 can require a completely integrated simulator that simultaneously analyzes the electromagnetic and circuit portions of the transformation exemplified by $\vec{H}_{EG}(f)$.

5.1.2. Pulse-sequence design

In the examples here, the pulse sequence generator produces patterns with Fourier transform $\Delta^{(d)}(f)$ given by (23). Assuming that mask-shape compliance can be achieved with reasonable efficiency by pulse-shape design, the sequence design producing $\Delta^{(d)}(f)$ for various values of d impacts sequence design in at least three possible ways.

Filling the regulatory mask

For this purpose, $|\Delta^{(d)}(f)|^2$ should be as flat a function of f as possible across the UWB bandwidth. The best designs for this purpose, using either time-hopping or direct-sequence modulation, most likely related to difference set designs [41].

[2] If this efficient design assumption is not valid or if the messages are not selected independently, see [10] for spectral calculations.

[3] Here $h_{EG}(t)$ can be viewed as any component of $\vec{h}_{EG}(t)$.

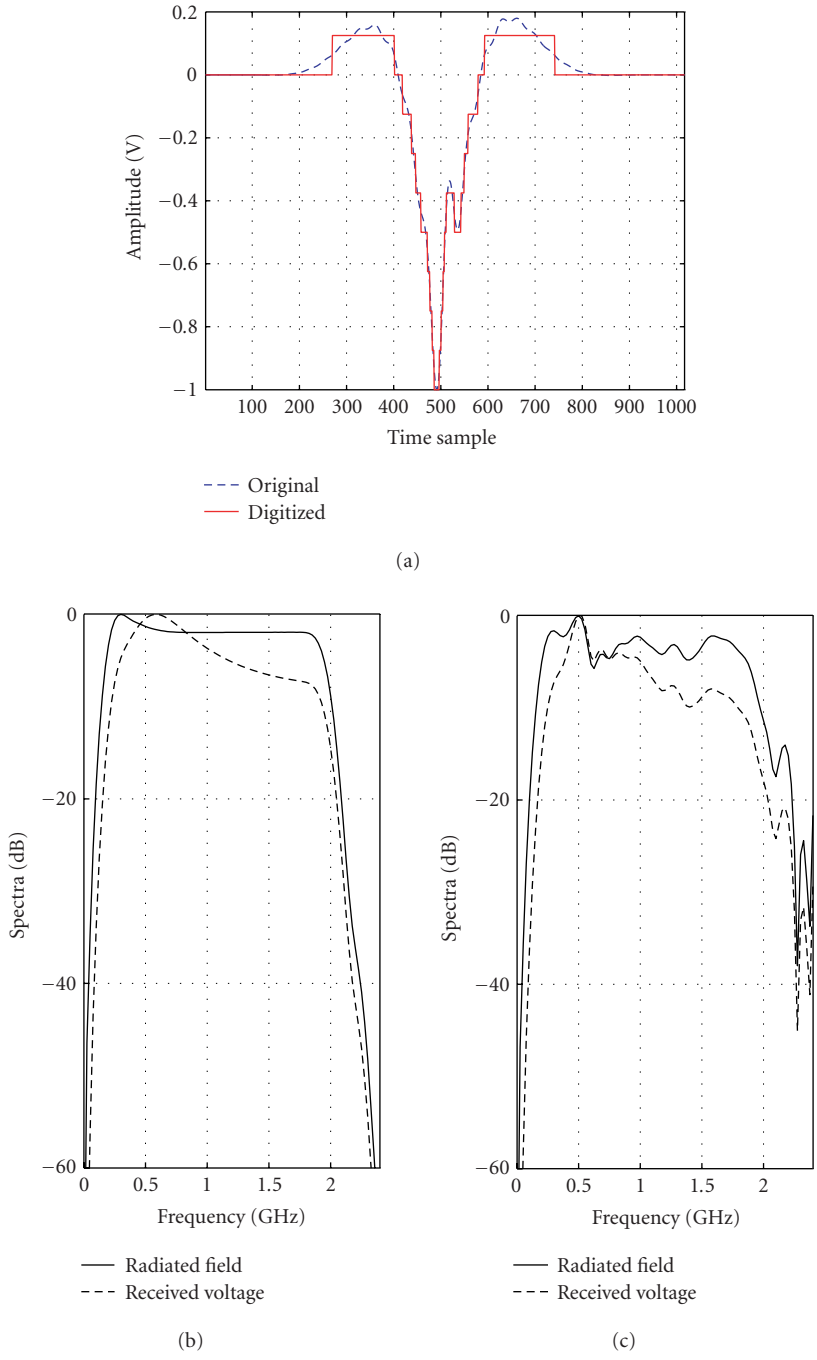

FIGURE 10: Quantization and spectral occupancy effects for a bow-tie antenna link. (a) Continuous and quantized source signal. (b) Normalized energy spectral densities of the radiated field (solid trace) and received signal (dashed trace) for the continuous source signal. (c) Normalized energy spectral densities of the radiated field (solid trace) and received signal (dashed trace) for the quantized source signal.

Designing synchronous orthogonal signals

The requirement for synchronous orthogonal signals is typically needed for data modulation so that a receiver can separate data symbol components using correlation techniques. Suppose that $H_{\mathrm{LG}}(f)$ is the system function of the linear transformation from the source voltage $v_{\mathrm{G}}(t)$ to the receiver load voltage $v_{\mathrm{L}}(t)$. In this situation when $v_{\mathrm{G}d}(t)$ and $v_{\mathrm{L}d}(t)$ are received, then

$$v_{\mathrm{L}m}(t) \perp v_{\mathrm{L}n}(t) \iff \int_{-\infty}^{\infty} v_{\mathrm{L}m}(t) v_{\mathrm{L}n}(t)\,dt = \int_{-\infty}^{\infty} \Delta^{(m)}(f)\left(\Delta^{(n)}(f)\right)^{*} \left|P_{\mathrm{G}}(f)\right|^{2} \left|H_{\mathrm{LG}}(f)\right|^{2} df = 0, \tag{26}$$

and this criterion cannot be simplified for close-packed pulse designs in which interpulse interference occurs in the receiver.

Designing asynchronous quasiorthogonal signals for multiple access

Pulse patterns can also be used in multiple-access systems for separation of signals from different transmitters. Since the transmitters clocks typically are not synchronous, asynchronous signal designs similar or identical to those used for direct-sequence spread-spectrum multiple access (DS-SSMA) must be used. It is quite likely that the models from the source voltages in these transmitters to the receiver load voltage will differ in some ways. In any event, the correlation properties of the received signals will depend on the basic pulse-shape voltages across the receiver load, as well as the outputs of the transmitters' pulse pattern generators. For more on DS-SSMA signal designs, see [42], and for time-hopping variations of these designs, see [41].

5.2. Receiver design: robust algorithms

The indoor environments in which UWB communication applications are contemplated often exhibit pulse response functions like those of Figure 3, that is, the delay spread of the multipath channel is much larger than the resolution capability of the signal being employed. In this situation, the resolved paths do not interfere with each other and the effects of fading are reduced (e.g., see [43, Table 1]).[4] However, the UWB receiver must be designed to learn and track changes in the pulse response function and use that information to efficiently demodulate the signal. This can be done with a baseband version of a RAKE receiver which combines the signals coming over resolvable propagation paths in a way that maximizes the energy-per-bit-to-noise density ratio. Suppose that $r(t)$ represents a received pulse waveform, and $r_{\text{temp}}(t)$ represents the pulse template to which a correlation detector is matched. Assume that antipodal modulation of N_{p} pulses is used to carry one data bit and that the pulses are far enough apart in time to prevent interpulse interference in the receiver. Then it can be shown that the uncoded bit error probability for this stored-reference (SR) correlation receiver is

$$P_{\text{eSR}} = Q\left(\sqrt{\frac{2E_{\text{p}}N_{\text{p}}\eta_{\text{capSR}}}{N_0}}\right), \tag{27}$$

where $Q(x) = (2\pi)^{-1/2}\int_{-\infty}^{\infty}\exp(-z^2/2)dz$, and generally

$$\eta_{\text{cap}} = \frac{\left[\int_{-\infty}^{\infty} r(t)r_{\text{temp}}(t)dt\right]^2}{\int_{-\infty}^{\infty} r^2(t)dt\int_{-\infty}^{\infty} r_{\text{temp}}^2(t)dt}, \qquad E_{\text{p}} = \int_{-\infty}^{\infty} r^2(t)dt. \tag{28}$$

[4]It should be noted that while the UWB signal fades caused by antenna movement are not large in most propagation environments, narrowband interference in the UWB receiver can fade or strengthen with relatively small movements of the receiving antenna.

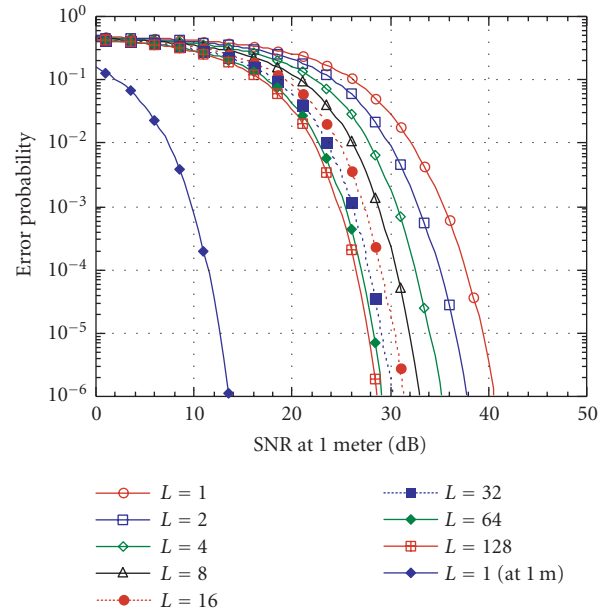

Figure 11: Performance of optimal selective RAKE combiner, as a function of the number L of signal components combined.

The quantity η_{cap} (η_{capSR} for the SR receiver) is called the *energy capture efficiency* of the receiver. As the energy capture efficiency η_{cap} decreases for a given available energy E_{p} per pulse, the probability P_{err} of error increases.

5.2.1. Selective RAKE receivers

A full RAKE receiver uses the signal components from all propagation paths, while a selective RAKE receiver performs this process on subset of the component signals. The performance of a selective RAKE receiver that optimally combines L paths can be calculated from measurements using (27) and (28) (see Figure 11). The receiver parameter L affects the performance because it affects the energy capture efficiency. The curves in Figure 11 are constructed from a set of measured pulse response functions corresponding to transmissions from a laboratory to an office across a hall. The path strengths and delays for a measurement were determined by a basic CLEAN algorithm similar to the one mentioned in Section 3.3, and the effective template used in the CLEAN algorithm was the same $r_{\text{temp}}(t)$ that was assumed to be used by the pulse correlator ($L = 1$) in the receiver. Note that the difference between using the strongest component path ($L = 1$) and essentially the whole pulse response function ($L = 128$) is roughly 10 + dB in bit-energy-to-noise power density ratio for reasonable operating points. This indicates that $\eta_{\text{capSR}} < 0.1$ for the set of measurements used to generate Figure 11.

5.2.2. Transmitted-reference systems

An alternative to a RAKE receiver's complexity is provided by a simple transmitted-reference (TR) system [44, 45] in which pulses are transmitted in pairs, one pulse $p(t)$ (the reference pulse) transmitted without data modulation, followed

at a fixed time delay τ_{del} later by a data modulated pulse $\pm p(t-\tau_{\text{del}})$. Hence, if N_{p} pulses are transmitted per bit, then $N_{\text{p}}/2$ serve as reference pulses that are interleaved with $N_{\text{p}}/2$ data-modulated (± 1) pulses. The receiver cross-correlates the reference pulse with the following data-modulated pulse, and the results of this correlation are accumulated over the $N_{\text{p}}/2$ pulse-pair transmissions that represent the same data bit. The advantage of this technique is that the noisy received reference pulse emulates the whole received pulse waveform, and the TR receiver in principle does not suffer from low energy-capture efficiency η_{capSR}. On the other hand, the gain in the energy-capture efficiency of this TR system can be offset by the fact that the reference template is noisy, with noise $\times$ noise products in the correlator causing performance degradation.

The performance of the TR system depends on two other parameters that do not appear in the idealized SR system performance model, namely, the one-sided RF bandwidth W and the duration T_{corr} of the pulse-correlation operation (which begins with the beginning of the signal component received over the direct propagation path). These parameters limit the noise that appears on both arms of the TR system correlator, but as T_{corr} is reduced below the received pulse length, the energy capture efficiency η_{capTR} of the TR receiver also decreases. The bit error probability for this simple TR system is approximately

$$P_{\text{eTR}} \approx Q\left(\left[\frac{2}{N_{\text{p}}}\left(\frac{N_0}{\eta_{\text{capTR}}E_{\text{p}}}\right)+\frac{WT_{\text{corr}}}{N_{\text{p}}}\left(\frac{N_0}{\eta_{\text{capTR}}E_{\text{p}}}\right)^2\right]^{-1/2}\right). \tag{29}$$

Here T_{corr} appears explicitly and also implicitly because it affects the energy-capture efficiency by limiting the range of integration of the correlator.

5.2.3. Comparisons of TR and SR systems

A rough comparison of simple transmitted- and stored-reference receivers (TR and SR) can be made using (27) and (29), with the result that

$$P_{\text{eTR}} < P_{\text{eSR}} \iff \frac{E_{\text{p}}}{N_0} > \frac{WT_{\text{corr}}}{\eta_{\text{capTR}}^2\left(1/2\eta_{\text{capSR}}-2/\eta_{\text{capTR}}\right)}. \tag{30}$$

Hence, the TR receiver cannot outperform the SR receiver at any pulse-energy-to-noise density ratio if $\eta_{\text{capTR}}/\eta_{\text{capSR}} < 4$. It is worth noting that this comparison does not depend on the number N_{p} of pulses employed, and is only a function of the pulse-correlation technique. Furthermore, when the TR system is better, it is better at high pulse-energy-to-noise density ratios, that is, the conditions under which the noise $\times$ noise terms in the TR correlator have little effect on performance, and the TR system has an energy-capture advantage. Furthermore, the comparison depends on the particular pulse waveform $r(t)$ (and hence channel realization) through the two capture efficiencies η_{capSR} and η_{capTR}.

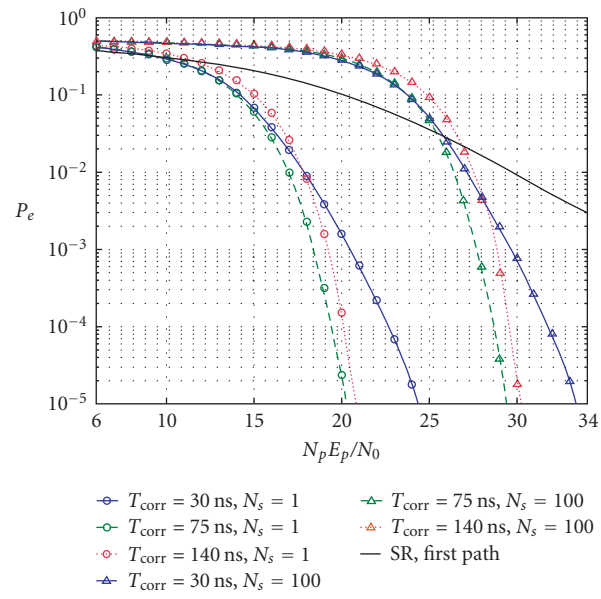

Figure 12: Comparison of TR- and SR-UWB systems. Note that $N_{\text{p}}E_{\text{p}}/N_0 = E_{\text{b}}/N_0$ is the bit-energy-to-noise-power density ratio, and $N_s = N_{\text{p}}/2$ is the number of pulse pairs used to represent a bit.

A comparison of uncoded bit error rate performance for an SR receiver using one signal component ($L = 1$) and a TR receiver is shown in Figure 12. These curves are based on (27) and (29) with identical parameters, except for the different energy-capture efficiencies, depending on L in the SR case and T_{corr} in the TR case. The performances shown here are of average over 1000 realizations of channel model CM4 adopted by modeling task force of the IEEE 802.15.3 Standards Committee [46]. In this computation, the source pulse-signal model is of the form $[1-4\pi(t/\sigma)^2]\exp(-2\pi t^2/\sigma^2)$, $\sigma \approx 0.29$ nanosecond, and $W = 2$ GHz. If the pulse is modified to be narrower in time, we expect the curves to move to the right for the following reasons: (a) the TR curves will move to the right because the RF bandwidth parameter W will increase, and (b) the SR curves will move to the right because more paths will be resolved, and on the average less pulse energy will be collected for a fixed value of the parameter L.

It is hard to make a fair comparison of TR- and SR-UWB receivers. Performance is only one of several parameters that must be compared for each system, for example, size, cost, power consumption, implementability, and so forth. The TR system is viewed as an alternate solution to the complexity of SR receivers using multifinger ($L > 1$) RAKE receivers, the TR receiver requiring one or at most a few short analog delay lines to implement values of the delay τ_{del}. This trades away TR system performance for various design costs. The result is that digital sampling and storage at a rate $(2W)^{-1}$ is not required in a simple TR receiver, and in principle the TR receiver may be simpler or cheaper to implement. It is also clear that there are ways to improve the simple UWB-TR receiver by reducing the noise in the reference waveform with

multiple-reference-pulse averaging of some sort. The cost of this improvement in TR systems typically is a way to store and process received UWB waveforms, considerably increasing the complexity, cost, and other parameters of the TR design. While these are legitimate radio designs, they should be compared more fairly to SR radios with the same general processing resources.

5.3. Sync acquisition with UWB channels

Often synchronization of signals propagated over AWGN channels can be viewed as an appropriately scaled version of bit (or code) sync algorithms of narrowband systems, quite possibly unencumbered by the problems of carrier synchronization. The major difference in the UWB-AWGN channel is the distortion of the source signal as it undergoes propagation through the antenna system (see Section 3.1.1). In a realistic indoor channel with relatively dense multipath (see Section 3.3), the signal acquisition system has the opportunity to synchronize with any of the multipath components of the received signal. This tends to make the acquisition time proportional to the ratio $T_{\text{unc}}/T_{\text{msp}}$ of the timing uncertainty interval to the multipath time spread, rather than $T_{\text{unc}}/T_{\text{res}}$ for simple AWGN channels (see Section 2.3).

To minimize the time for the receiver to synchronize to any one of the available signal components, a serial search should ideally compute the likelihood of the delay at which a component exists, and attempt to lock at the most likely component delay, updating the likelihood profile after each synchronization attempt [17]. Because the multipath components tend to cluster in time, an approximation to this optimal rule is to look at prospective path delays that are as far as possible in delay from prior unsuccessful tests. A search approach that implements this without knowledge of the multipath spread T_{msp} has been designed using a technique called a bit-reversal search [47, 48], and its performance evaluated, based on real channel pulse response profiles.

Initial acquisition of a UWB signal component in multipath may be viewed as a first step, that is, coarse synchronization. The subsequent fine synchronization process has the objective of determining the delays and amplitudes of other multipath signal components, which can serve several objectives: (a) to find the strongest signal component (or components) for use in a simple (or RAKE) receiver, (b) to completely characterize the multipath channel, or (c) to find the earliest arriving signal component (presumably the direct path) for use in ranging or time-transfer systems. Simple statistical models for the time and amplitude relationship between the direct path and strongest path components of the received signal have been developed from indoor office/laboratory building measurements, and used in range measurements [49] (see also Ultra Lab website). Interestingly, the results demonstrated that ranging errors were on the order of fractions of a pulse width for clear LOS communications in agreement with the results of Section 2.3, but ranging errors for other situations were dominated by propagation anomalies, for example, propagation blockages, reduction of propagation speed through materials, and the inability to identify the LOS signal component.

6. FINDING A NICHE FOR UWB

So, when all is said, what are the applications for UWB communications? Is there a capability possessed only by UWB radio systems that leads to the so-called "killer" application for which there is no competing technology with comparable performance? Some are betting that it will be very short-range high data-rate applications, a potentially big commercial market, for example, wireless personal area networks (WPANs) [50, 51]. Comparisons in [50] indicate that the *spatial efficiency* of UWB systems (estimated at 1 000 000 bits/second/square meter) far exceeds efficiencies of systems based on the IEEE802.11a Standard (estimated at 83 000 bits/second/square meter), Bluetooth (estimated at 30 000 bits/second/square meter), and the IEEE802.11b Standard (estimated at 1000 bits/second/square meter). Capacity calculations for AWGN-UWB channels support this assessment.

High data-rate systems are not the only possible application. In addition to WPANs and other high-rate applications, the broader view given in [52] cites a "wide range of novel wireless communications" as possibilities, including vehicle collision avoidance, public safety systems (including motion detection applications), RF tags for personnel and asset tracking, location-aware ad hoc networking taking advantage of the position measurement capabilities of UWB technology, and so forth. This emphasis on ranging and radar imaging has been the foundation of much prior work on military applications, and has been called out as the basis for commercial killer applications [53]. The technological feasibility of these applications is motivated by the promises UWB radio discussed in Section 2.

UWB technology has progressed well beyond the point of demonstrating the feasibility of many of these applications. But experience with UWB consumer end-products in the field is still a thing of the future. Lack of agreement on a UWB standard at the time of this writing can be interpreted as a reflection of this lack of experience, or more likely a battle over UWB intellectual property. Whatever the reason, these are interesting times for engineers working on UWB communications.

ACKNOWLEDGMENTS

The authors wish to thank the following for their assistance in putting this tutorial together: Professor Dan Schaubert and Dr. Anatoliy Boryssenko of the University of Massachusetts at Amherst for generating transient data for the log-periodic and Vivaldi antennas, and also for providing the simulation graphics on signal quantization and spectral occupancy in Figure 10; Yi-Ling Chao, a Ph.D. candidate at USC, for the comparison of UWB-TR and -SR receivers illustrated in Figure 12; the International Society for Optical Engineering for permission to reprint Figure 2 in this paper from [16]; Jeff Foerster for providing useful information and comments, and graduate students at the University of Southern California for many useful discussions of UWB radio systems. This work was supported by the US Army Research Office under MURI Contract DAAD19-01-1-0477.

REFERENCES

[1] T. W. Barrett, "History of ultrawideband (UWB) radar & communications: pioneers and innovators," in *Progress in Electromagnetics Symposium (PIERS '00)*, Cambridge, Mass, USA, July 2000.

[2] B. Noel, Ed., *Ultra-Wideband Radar: Proceedings of the First Los Alamos Symposium*, CRC Press, Boca Raton, Fla, USA, 1991.

[3] H. Bertoni, L. Carin, and L. Felsen, Eds., *Ultra-Wideband Short-Pulse Electromagnetics*, Plenum Press, New York, NY, USA, 1993.

[4] L. Carin and L. Felsen, Eds., *Ultra-Wideband Short-Pulse Electromagnetics 2*, Plenum Press, New York, NY, USA, 1995.

[5] C. Baum, L. Carin, and A. Stone, Eds., *Ultra-Wideband Short-Pulse Electromagnetics 3*, Plenum Press, New York, NY, USA, 1997.

[6] E. Heyman, B. Mandelbaum, and J. Shiloh, Eds., *Ultra-Wideband Short-Pulse Electromagnetics 4*, Kluwer Academic/Plenum Press, New York, NY, USA, 1999.

[7] P. Smith and S. Cloude, Eds., *Ultra-Wideband, Short-Pulse Electromagnetics 5*, Kluwer Academic/Plenum Press, New York, NY, USA, 2002.

[8] Federal Communications Commission (FCC), "Revision of part 15 of the commission's rules regarding ultra-wideband transmission systems," First Report and Order, ET Docket 98–153, FCC 02–48; Adopted: February 2002; Released: April 2002.

[9] Federal Communications Commission (FCC), "Revision of part 15 of the commission's rules regarding ultra-wideband transmission systems," Memorandum Opinion and Order and Further Notice of Proposed Rule making, ET Docket 98–153, FCC 03–33; Adopted:February 2003; Released:March 2003.

[10] R. A. Scholtz, "How do you define bandwidth?," in *Proc. International Telemetering Conference*, pp. 281–288, Los Angeles, Calif, USA, October 1972.

[11] J. M. Wozencraft and I. M. Jacobs, *Principles of Communication Engineering*, John Wiley & Sons, New York, NY, USA, 1965.

[12] C. E. Shannon, "Communication in the presence of noise," *Proceedings of the IRE*, vol. 37, no. 1, pp. 10–21, 1949.

[13] R. A. Scholtz, "The spread spectrum concept," *IEEE Trans. Communications*, vol. 25, no. 8, pp. 748–755, 1977.

[14] R. A. Scholtz, R. Weaver, E. Homier, et al., "UWB radio deployment challenges," in *Proc. IEEE International Symposium on Personal, Indoor and Mobile Radio Communications (PIMRC '02)*, vol. 1, pp. 620–625, London, UK, September 2000.

[15] J.-Y. Lee and R. A. Scholtz, "Problems in modeling ultra-wideband channels," in *Asilomar Conference on Signals, Systems, and Computers*, Pacific Grove, Calif, USA, November 2002.

[16] L. M. Frazier, "Radar surveillance through solid materials," in *Command, Control, Communications, and Intelligence Systems for Law Enforcement*, vol. 2938, pp. 139–146, Boston, Mass, USA, November 1996.

[17] J. J. Stiffler, *Theory of Synchronous Communications*, Prentice-Hall, Englewood Cliffs, NJ, USA, 1971.

[18] J. R. Andrews, "UWB signal sources, antennas & propagation," Application note AN-14a, Picosecond Pulse Labs, Boulder, Colo, USA, August 2003.

[19] J. A. N. Noronha, T. Bielawa, C. R. Anderson, D. G. Sweeney, S. Licul, and W. A. Davis, "Designing antennas for UWB systems," *Microwaves & RF Magazine*, pp. 53–61, June 2003.

[20] W. Sorgel, C. Waldschmidt, and W. Wiesbeck, "Transient responses of a Vivaldi antenna and a logarithmic periodic dipole array for ultra wideband communication," in *IEEE International Symposium on Antennas and Propagation*, vol. 3, pp. 592–595, Columbus, OH, USA, June 2003.

[21] L. B. Felsen, Ed., *Transient Electromagnetic Fields*, Springer-Verlag, New York, NY, USA, 1976.

[22] J. G. Maloney, G. S. Smith, and W. R. Scott Jr., "Accurate computation of the radiation from simple antennas using the finite-difference time-domain method," *IEEE Trans. Antennas Propagat.*, vol. 38, no. 7, pp. 1059–1068, 1990.

[23] D. M. Pozar, "Waveform optimizations for ultrawideband radio systems," *IEEE Trans. Antennas Propagat.*, vol. 51, no. 9, pp. 2335–2345, 2003.

[24] D. M. Pozar, "Closed-form approximations for link loss in a UWB radio system using small antennas," *IEEE Trans. Antennas Propagat.*, vol. 51, no. 9, pp. 2346–2352, 2003.

[25] C. A. Balanis, *Antenna Theory: Analysis and Design*, John Wiley & Sons, New York, NY, USA, 2nd edition, 1997.

[26] R. J.-M. Cramer, R. A. Scholtz, and M. Z. Win, "Evaluation of an ultra-wide-band propagation channel," *IEEE Trans. Antennas Propagat.*, vol. 50, no. 5, pp. 561–570, 2002.

[27] J. Kunisch and J. Pamp, "Measurement results and modeling aspects for the UWB radio channel," in *IEEE Conference on Ultra Wideband Systems and Technologies*, pp. 19–23, Baltimore, Md, USA, May 2002.

[28] S. S. Ghassemzadeh, R. Jana, C. W. Rice, W. Turin, and V. Tarokh, "A statistical path loss model for in-home UWB channels," in *IEEE Conference on Ultra Wideband Systems and Technologies*, pp. 59–64, Baltimore, MD, USA, 2002.

[29] D. Cassioli, M. Win, and A. Molisch, "The ultra-wide bandwidth indoor channel: from statistical model to simulations," *IEEE J. Select. Areas Commun.*, vol. 20, no. 6, pp. 1247–1257, 2002.

[30] A. F. Molisch, J. R. Foerster, and M. Pendergrass, "Channel models for ultrawideband personal area networks," *IEEE Wireless Communications*, vol. 10, no. 6, pp. 14–21, 2003.

[31] A. Saleh and R. Valenzuela, "A statistical model for indoor multipath propagation," *IEEE J. Select. Areas Commun.*, vol. 5, no. 2, pp. 128–137, 1987.

[32] Q. Spencer, M. Rice, B. Jeffs, and M. Jensen, "Indoor wideband time/angle of arrival multipath propagation results," in *Proc. IEEE Vehicular Technology Conference (VTC '97)*, pp. 1410–1414, Phenix, Ariz, USA, 1997.

[33] A. Batra, J. Balakrishnan, A. Dabak, et al., "Multi-band OFDM physical layer proposal for IEEE 802.15 Task Group 3a," IEEE 802.15-03/268r2, November 2003.

[34] W. Namgoong, "A channelized digital ultrawideband receiver," *IEEE Transactions on Wireless Communications*, vol. 2, no. 3, pp. 502–510, 2003.

[35] L. Feng and W. Namgoong, "An oversampled channelized UWB receiver," in *Proc. IEEE Conference on Ultrawideband Systems and Technologies (UWBST '04)*, pp. 410–414, Kyoto, Japan, May 2004.

[36] L. Feng and W. Namgoong, "Oversampled channelized receiver for transmitted reference UWB system in the presence of narrowband intererence," in *IEEE Workshop on Signal Processing Systems*, Kyoto, Japan, May 2004.

[37] L. Feng and W. Namgoong, "An adaptive maximally decimated channelized UWB receiver with cyclic prefix," in *IEEE International Conference on Communications*, Seoul, Korea, May 2005.

[38] W. Namgoong and J. Lerdworatawee, "Noise figure of digital communication receivers-revisited," *IEEE Transactions on Circuits and Systems I: Regular Papers*, vol. 51, no. 7, pp. 1330–1335, 2004.

[39] S. Andersson, C. Svensson, and O. Drugge, "Wideband LNA for a multistandard wireless receiver in 0.18 μm CMOS," in *Proc. Conference on European Solid-State Circuits (ESSCIRC '03)*, pp. 655–658, Estoril, Portugal, September 2003.

[40] A. Bevilacqua and A. M. Niknejad, "An ultra-wideband CMOS LNA for 3.1 to 10.6 GHz wireless receivers," in *IEEE International Solid-State Circuits Conference (ISSCC '04)*, vol. 1, pp. 382–533, San Francisco, CA, USA, February 2004.
[41] R. A. Scholtz, P. V. Kumar, and C. Corrada-Bravo, "Some problems and results in ultra-wideband signal design," in *Sequences and Their Applications (SETA '01)*, Bergen, Norway, May 2001.
[42] M. Simon, J. Omura, R. Scholtz, and B. Levitt, *Spread Spectrum Communications Handbook*, McGraw-Hill, New York, NY, USA, 1994.
[43] R. A. Scholtz and M. Z. Win, "Impulse radio," in *Wireless Communications: TDMA versus CDMA*, S. Glisic and P. Leppänen, Eds., pp. 1677–1683, Kluwer Academic Publishers, Boston, Mass, USA, September 1997.
[44] C. K. Rushforth, "Transmitted-reference techniques for random or unknown channels," *IEEE Trans. Inform. Theory*, vol. 10, no. 1, pp. 39–42, 1964.
[45] R. T. Hoctor and H. W. Tomlinson, "An overview of delay-hopped, transmitted-reference RF communications," Tech. Rep., General Electric Research and Development Center, Niskayuna, NY, USA, January 2002.
[46] J. Foerster, "Channel modeling sub-committee report final," IEEE P802.15-02/368r5-SG3a, December 2002, http://ieee802.org/15/.
[47] E. Homier and R. A. Scholtz, "Hybrid fixed-dwell-time search techniques for rapid acquisition of ultra-wideband signals," in *International Workshop on Ultrawideband Systems (IWUWBS '03)*, Oulu, Finland, June 2003.
[48] E. Homier and R. A. Scholtz, "A generalized signal flow graph approach for hybrid acquisition of ultra-wideband signals," *International Journal of Wireless Information Networks*, vol. 10, no. 4, pp. 179–191, 2003.
[49] J.-Y. Lee and R. A. Scholtz, "Ranging in a dense multipath environment using an UWB radio link," *IEEE J. Select. Areas Commun.*, vol. 20, no. 9, pp. 1677–1683, 2002.
[50] J. Foerster, E. Green, S. Somayazulu, and D. Leeper, "Ultra-wideband technology for short- or medium-range wireless communications," *Intel Technology Journal*, Q2, 2001.
[51] S. Roy, J. R. Foerster, V. S. Somayazulu, and D. G. Leeper, "Ultrawideband radio design: the promise of high-speed, short-range wireless connectivity," *Proc. IEEE*, vol. 92, no. 2, pp. 295–311, 2004.
[52] W. Hirt, "Ultra-wideband radio technology: overview and future research," *Computer Communications*, vol. 26, no. 1, pp. 46–52, 2003.
[53] USC Communication Sciences Institute, "Workshop on ultrawideband radio techniques," Los Angeles, Calif, USA, May 1998.

Robert A. Scholtz is the Fred H. Cole Professor of engineering at the University of Southern California. In 1996, he founded the Ultrawideband Radio Laboratory (UltRa Lab) there. His research interests include communication theory, synchronization, signal design, adaptive processing, pseudonoise generation, and ultra-wideband radio. He has coauthored *Spread Spectrum Communications* (Computer Science Press), *Spread Spectrum Communications Handbook* (McGraw-Hill), and *Basic Concepts in Information Theory and Coding* (Plenum). Dr. Scholtz is a Fellow of the IEEE. He received the 1983 Leonard G. Abraham Prize and the 1984 Donald G. Fink Prize for the historical article, "The origins of spread spectrum communications." He is a corecipient of the 1992 Senior Award of the IEEE Signal Processing Society, the 1997 Ellersick Award from MilCom, the 2003 S. A. Schelkunoff Prize from the IEEE Antennas and Propagation Society, and Best Paper Award at the 2003 International Workshop on Ultrawideband Systems, the latter two for works on UWB radio. In 2001, he received the Military Communications Conference Award for Technical Achievement. He has been General Chairman of six workshops in the area of communications, including most recently two ultra-wideband radio workshops held in May 1998 and October 2002 (the latter jointly with Intel).

David M. Pozar received the Ph.D. degree from Ohio State University, and joined the faculty at the University of Massachusetts in 1980. In 1988, he spent a sabbatical leave at École Polytechnique Fédérale de Lausanne, Lausanne, Switzerland. Professor Pozar is a Fellow of the IEEE. He has served as an Associate Editor of the IEEE Transactions on Antennas and Propagation (1983–1986 and 1989–1992), as a Member of the IEEE AP-S AdCom (1989–1991), and as an Associate Editor of the IEEE AP-S Newsletter (1982–1984). In 1981, he received the Outstanding Professor for 1981 Award from Eta Kappa Nu, the Student Honor Society. In 1984, he received an NSF Presidential Young Investigator Award, and the Keys to the Future Award from the IEEE Antennas and Propagation Society. In 1985, he received the University of Massachusetts Engineering Alumni Association Outstanding Junior Faculty Award. In 1986, he received the R.W.P. King Best Paper Award from the IEEE Antennas and Propagation Society. In 1987, he received the URSI Issac Koga Gold Medal for his work on printed antennas and phased arrays. He again received the R.W.P. King Best Paper Award in 1988. In 1989, he received the United Technologies Corporation Outstanding Teaching Award. He served as a Distinguished Lecturer for the IEEE Antennas and Propagation Society in 1993–1995. In 1995, he received the College of Engineering Outstanding Senior Faculty Award. He received the College of Engineering College Outstanding Teacher Award in 1997. In 1998, he received the H. A. Wheeler Applications Prize Paper Award from IEEE Antennas and Propagation Society. He received an IEEE Third Millennium Medal in 2000. In 2003, he received the S. A. Schelkunoff Transactions Prize Paper Award from the IEEE Antennas and Propagation Society, as well as the Chancellor's Medal from the University of Massachusetts, and was a Distinguished Faculty Lecturer at the University of Massachusetts. Professor Pozar has published over 100 papers on microstrip antennas and phased arrays, and is the author of *Microwave Engineering, 3rd edition* (Wiley, 2004), *Microstrip Antennas* (IEEE Press, 1995), and *Microwave and RF Design of Wireless Systems* (Wiley, 2000).

Won Namgoong received the B.S. degree in electrical engineering and computer science from the University of California at Berkeley in 1993, and the M.S. and Ph.D. degrees in electrical engineering from Stanford University in 1995 and 1999, respectively. In 1999, he joined the faculty of the Electrical Engineering Department, the University of Southern California, where he is an Assistant Professor. His current research areas include wireless/wireline communication systems, signal processing systems, RF circuits, and low-power/high-speed circuits. In 2002, he received the National Science Foundation (NSF) CAREER Award. He currently serves as the Associate Editor of IEEE Transactions on Circuits and Systems I—Regular Papers.